UCRL-18141 Rev.
cy.2

University of California

Ernest O. Lawrence Radiation Laboratory

ETA PRODUCTION IN THE REACTION $\pi p \rightarrow \pi p \eta$ AT 1050 AND 1170 MeV/c

Ronald A. Grossman, LeRoy R. Price, and Frank S. Crawford, Jr.

June 5, 1968

UCRL-18141 Rev.
cy.2

E,P

DISCLAIMER

Submitted to Physical Review

UCRL-18141 Rev.
Preprint

UNIVERSITY OF CALIFORNIA

Lawrence Radiation Laboratory
Berkeley, California

AEC Contract No. W-7405-eng-48

ETA PRODUCTION IN THE REACTION $\pi p \rightarrow \pi p \eta$ AT 1050 AND 1170 MeV/c

Ronald A. Grossman, LeRoy R. Price, and Frank S. Crawford, Jr.

June 5, 1968

ETA PRODUCTION IN THE REACTION $\pi p \rightarrow \pi p \eta$ AT 1050 AND 1170 MeV/c*

Ronald A. Grossman, LeRoy R. Price, and Frank S. Crawford, Jr.

Lawrence Radiation Laboratory
University of California
Berkeley, California

June 5, 1968

ABSTRACT

We have investigated eta production in the reaction $\pi^+ p \rightarrow \pi^+ p \eta$ at 1050 and 1170 MeV/c, and in the reaction $\pi^- p \rightarrow \pi^- p \eta$ at 1170 MeV/c. We obtain the following partial cross sections for the reaction $\pi^{\pm} p \rightarrow \pi^{\pm} p \eta$ followed by the charged decay $\eta \rightarrow \pi^+ \pi^- \pi^0$: (9.5 ± 1.5) μb for 1050 MeV/c incident π^+; (53.3 ± 5.0) μb for 1170 MeV/c π^+; (15.9 ± 1.9) μb for 1170 MeV/c π^-. From our π^+ data we find that we need four I = 3/2 amplitudes in order to obtain good agreement with our mass and angular distributions and to reproduce the threshold behavior of the cross section. We find the dominating amplitude to be that representing the reaction, $\pi^+ p \rightarrow \eta \Delta(1238)$; $\Delta(1238) \rightarrow \pi^+ p$, where the η and the $\Delta(1238)$ are produced in s-wave. The four amplitudes are extrapolated to higher energies where the predicted mass and angular distributions and cross sections are compared with the available data. From our π^- data we find that in addition to the four I = 3/2 amplitudes (determined from the π^+ data), one I = 1/2 amplitude is required: the amplitude in which all particles are in relative S-states. We find that this I = 1/2 amplitude in fact dominates the π^- reaction. We see no evidence for production of an $N^*(1550) \rightarrow \eta p$ resonance. We are able to parameterize the cross sections for $\pi p \rightarrow \pi p \eta$ from threshold to 4 BeV/c.

I. INTRODUCTION

Since the discovery of the eta meson in 1961,[1] there have been several experiments[2-7] at various energies involving the reaction $\pi^+ p \rightarrow \pi^+ p\eta$. In all of these experiments the reaction appears to proceed mainly via

$$\pi p \rightarrow \eta\, \Delta(1238)$$
$$\Delta(1238) \rightarrow \pi p. \qquad (1)$$

There have also been a few experiments[8-10a] involving the reaction $\pi^- p \rightarrow \pi^- p\eta$.

Reaction (1) is unusual in that there are no pseudoscalar or vector mesons which can be exchanged in the t-channel. Therefore, such models as the one pion exchange model or the vector exchange model of Stodolsky and Sakurai[11] do not apply to reaction (1). As can be seen from the figure below,

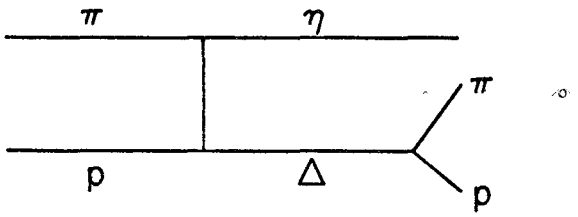

the required quantum numbers for the exchange particle are $I^G = 1^-$ and $J^P = 0^+, 1^-, 2^+, \cdots$. Possible mesons with these quantum numbers are the massive $A_2(1300)$, $J^P = 2^+$; and $\pi_V(1016)$, $J^P = 0^+$.

The A_2 meson is well established, and the quantum numbers are now fairly well agreed upon. (There is some evidence, however, that there might be more than one meson in this region.[12]) The compiled branching ratio for A_2 decay into $\eta\pi$ is listed[13] as $11 \pm 2\%$, indicating that the coupling constant at the upper vertex is small.

The other meson candidate for the exchange particle, $\pi_V(1016)$,[13] is seen as a $\bar{K}K$ enhancement near threshold and may be interpreted as due to a large scattering length. A reported $\eta\pi$ enhancement[14] in this region has not been confirmed.

In addition to meson exchange in the t-channel, it is also possible to have baryon exchange in the u-channel. This would tend to peak the backward region of the production angular distribution. For baryon exchange, the nucleon and the $N^*(1550)$, S_{11} resonance have the required quantum numbers.

The fact that the masses of all the proposed exchange particles are large has the consequence that the interaction is of shorter range than interactions to which the peripheral model is usually applied. It is not surprising, therefore, that experiments involving reaction (1) are not highly peripheral; that is, the production angular distributions do not exhibit the great forward peaking characteristic of peripheral interactions. In fact, in the low-energy data of Foelsche and Kraybill[2] and of this experiment, the production angular distributions are fairly flat.

We also note that in addition to $\Delta(1238)$ production the reaction $\pi p \to \pi p \eta$ might proceed via

$$\pi p \to \pi N^*(1550)$$

$$N^*(1550) \to \eta p.$$

In this paper we adopt the phenomenological approach of describing the production process of the reaction $\pi p \to \pi p \eta$ in terms of low partial waves. We find that our π^+ data at 1050 and 1170 MeV/c may be adequately represented by s-wave production of the eta and $\Delta(1238)$, plus

an admixture in which the eta is produced in s- or p-wave and the π^+ and p are in a relative S-wave. At 1170 MeV/c we find the cross section ratio $\sigma(\pi^- p \to \pi^- p\eta)/\sigma(\pi^+ p \to \pi^+ p\eta) = 0.30 \pm 0.04$ instead of the value 0.11 expected (on the basis of Clebsch-Gordan factors) if the $\pi^- p$ reaction proceeded only through the I = 3/2 amplitudes. This indicates that in addition to the I = 3/2 amplitudes there is also an appreciable I = 1/2 contribution. Our π^- data is adequately represented by the addition of only one I = 1/2 amplitude; the amplitude in which all particles are in relative S-states.

II. EXPERIMENTAL DETAILS

The Alvarez 72-inch liquid-hydrogen bubble chamber was exposed to beams of both π^+ and π^- mesons at a momentum of 1170 MeV/c and to π^+ mesons at a momentum of 1050 MeV/c. The beam setup has been described previously;[15, 16] we present here in Fig. 1 only a schematic diagram of the beam optics.

A total of 240 000 pictures were taken at the three momenta. The film was scanned for 4-prongs. A total of 14 000 4-prongs were found and fitted by the LRL spatial reconstruction and kinematical fitting program SIOUX. Most of the events, 12 000, fit the four-constrained reaction,

$$\pi^\pm p \to \pi^\pm p \pi^+ \pi^- \qquad (2)$$

with a chi-square less than 16. These events were discarded. The remaining 2000 events were then examined on the scanning table to determine the proton. Out of these 2000 events, 800 fit reaction (2) with a chi-square between 16 and 35. For these events, if the proton identifi-

cation made on the scanning table agreed with the track identified as the proton in the 4C fit of reaction (2), then the event was discarded. In addition, events identified on the scanning table as having Dalitz pairs and events identified as having four charged pions were also discarded.

The remaining events were retained if they fit the reaction

$$\pi^{\pm} p \rightarrow \pi^{\pm} p \pi^{+} \pi^{-} \pi^{0}$$

or

$$\pi^{\pm} p \rightarrow \pi^{\pm} p \pi^{+} \pi^{-} \gamma$$

with a one-constrained (1C) chi-square of less than 8.6 and if the events were inside the fiducial volume. The distributions in the missing neutral mass for these events are shown in Fig. 2. These events were then fit to the two-vertex, two-constrained hypothesis

$$\pi^{\pm} p \rightarrow \pi^{\pm} p \eta$$
$$\eta \rightarrow \pi^{+} \pi^{-} \pi^{0} \qquad (3)$$

and

$$\pi^{\pm} p \rightarrow \pi^{\pm} p \eta$$
$$\eta \rightarrow \pi^{+} \pi^{-} \gamma. \qquad (4)$$

An event was recorded as reaction (3) or (4) depending on which had the lower chi-square. Events fitting reaction (4) are not used. All but four of the events that fit $\pi^{\pm} p \rightarrow \pi^{\pm} p \pi^{+} \pi^{-} \pi^{0}$ also fit the 2C reaction (3) with chi-squares less than 20 and are regarded as good eta events. The four exceptions have chi-squares over 200. Thus, essentially all events which fit the final state hypothesis, $\pi p \pi^{+} \pi^{-} \pi^{0}$, come from etas. The number of events fitting reaction (3) are 135 for the 1170 MeV/c π^{+} data, 51 for the 1050 MeV/c π^{+} data, and 87 for the 1170 MeV/c π^{-}

data.[17] The 2C χ^2 distribution of these 273 events is given in Fig. 3.

There is still the problem of "ambiguous" events. As there are two pions of the same charge in the final state, it is unknown which pion has come from the decay of the eta; thus reaction (3) can be fitted two ways. When both fits are good (chi-square less than 20), the event is ambiguous. In this case, the interpretation with the lower chi-square is taken to be the correct one. In the analysis which follows it is assumed that the right identification is always made. (By a Monte Carlo calculation we estimate that we choose the wrong pion about 3% of the time.)

Another possible way in which we could have obtained our final sample of events—$\pi^{\pm} p \rightarrow \pi^{\pm} p\eta$, $\eta \rightarrow \pi^{+}\pi^{-}\pi^{0}$—is to separate out the events with a missing γ ray by taking all events in which the mass of the missing neutral is greater than 0.010 BeV^2 (see Fig. 2), and then plot the invariant mass of the $\pi^{+}\pi^{-}\pi^{0}$. The resulting plots are shown in Fig. 4. Again, because of the pion ambiguity, there are two such combinations; only the one in which the invariant mass is closer to the eta mass has been plotted. It is seen in Fig. 4 that this procedure likewise results in nearly all events being etas. This procedure is more visually appealing than the χ^2 method. We use the χ^2 criteria, however, because it takes measurement errors into account systematically and because, using the Monte Carlo program FAKE[18] we can more easily calculate the effects of cutoffs based on χ^2 than those based on calculated errors in missing mass.

III. CROSS SECTIONS

The measured cross sections for the reaction $\pi p \rightarrow \pi p \eta$, $\eta \rightarrow \pi^+\pi^-\pi^0$ for each of our three beams are given in Table I along with the pertinent scanning information.

As stated in Section II, an eta event is obtained by insisting that the 4C chi-square for "nothing missing" is greater than 35, that the 1C chi-square for missing π^0 or missing γ is less than 8.6, and that the 2C chi-square for eta decaying into $\pi^+\pi^-\pi^0$ is less than for the decay into $\pi^+\pi^-\gamma$. The last criterion introduces some misinterpretations if both chi-squares are small. In order to obtain the efficiency of the above selection criteria, FAKE was used to simulate events of type (3). The efficiency was found to be 91.5%. In addition, events of type (4) were faked. It was found that the number of $\pi^+\pi^-\gamma$ eta decays contaminating our final sample is negligible (less than 0.8 event).

The partial cross sections obtained in this experiment for reaction (3) are listed in Table II along with the cross section values given in references (2-10). A plot of these values as a function of incident beam momentum is shown in Fig. 5. Note that the ratio $\sigma(\pi^-p \rightarrow \pi^-p\eta)/\sigma(\pi^+p \rightarrow \pi^+p\eta)$ at 1170 MeV/c is $(15.9 \pm 1.9)/(53.3 \pm 5.0) = 0.30 \pm 0.04$. Were the π^-p reaction to proceed via I = 3/2 amplitudes only, such as through the reaction $\pi^-p \rightarrow \eta\Delta(1238)$, the ratio would be 1/9 = 0.11. Thus I = 1/2 amplitudes are important at 1170 MeV/c.

IV. EXPERIMENTAL DISTRIBUTIONS

A. Coordinate System

In the analysis which follows we regard the reaction $\pi^{\pm} p \to \pi^{\pm} p\eta$ as the two-step process:

$$\pi^{\pm} p \to \eta \tilde{N}$$

followed by

$$\tilde{N} \to \pi^{\pm} p,$$

where we use the symbol $\tilde{N}$ to indicate a π-p state of total angular momentum J and orbital angular momentum L. Thus when $J = 3/2$ and $L = 1$, $\tilde{N}$ corresponds to the $\Delta(1238)$.

Figure 6 is a mnemonic diagram in velocity space depicting the two-step process.[20] The beam pion π_B and target proton p_T of orbital angular momentum $\underset{\sim}{\mathcal{L}}$ and linear momentum $\underset{\sim}{k}$ in the overall center of mass of energy E produce an eta and a $\tilde{N}$ of orbital angular momentum $\underset{\sim}{\ell}$ and linear momentum $\underset{\sim}{p}$ in the overall center of mass. The $\tilde{N}$ of total angular momentum J then decays with orbital angular momentum $\underset{\sim}{L}$ and linear momentum $\underset{\sim}{q}$ in the $\tilde{N}$ rest frame. The total angular momentum of the system is $\underset{\sim}{\mathcal{J}}$. The final state $\pi^+ p\eta$ then consists of $I = 3/2$ states, $(\ell\ L_J)_{\mathcal{J}}$, and the final state $\pi^- p\eta$ consists of both $I = 3/2$ and $I = 1/2$ states, $(\ell\ L_J)_{\mathcal{J}}$. The notation is summarized in the following table.

	Particles		Linear momentum	Orbital ang. mom.	Total ang. mom.	energy
Initial (overall center of mass)	π_B,	p_T	$\underset{\sim}{k}$	$\underset{\sim}{\mathcal{L}}$	$\underset{\sim}{\mathcal{J}}$	E
Final (overall center of mass)	η ,	$\tilde{N}$	$\underset{\sim}{p}$	$\underset{\sim}{\ell}$	$\underset{\sim}{\mathcal{J}}$	E
$\tilde{N}$ rest frame	π_D,	p_D	$\underset{\sim}{q}$	$\underset{\sim}{L}$	$\underset{\sim}{J}$	M

We choose as the z axis the line of flight of the beam particle in the center of mass; that is,

$$\hat{z} = \frac{\underset{\sim}{k}}{|\underset{\sim}{k}|} .$$

We now define ξ as the angle in the center of mass between the line of flight of the eta and the line of flight of the incoming pion; that is,

$$\cos \xi = \frac{\underset{\sim}{p} \cdot \underset{\sim}{k}}{|\underset{\sim}{p}||\underset{\sim}{k}|} = \hat{p} \cdot \hat{z} .$$

The vectors $\underset{\sim}{p}$ and $\underset{\sim}{k}$ define the production plane. The y axis is defined as the normal to the production plane,

$$\hat{y} = \hat{n} = \frac{\underset{\sim}{k} \times \underset{\sim}{p}}{|\underset{\sim}{k}||\underset{\sim}{p}| \sin \xi} ;$$

and the x axis is defined so as to construct a right-handed coordinate system, $\hat{x} = \hat{y} \times \hat{z}$.

We now go to the $\tilde{N}$ rest frame and define the angles θ and ϕ as the polar and azimuthal angles of the decay proton:

$$\cos \theta = \hat{q} \cdot \hat{z},$$

$$\phi = \tan^{-1} [\hat{q} \cdot \hat{n} / \hat{q} \cdot \hat{x}] .$$

In this frame the z axis is defined to be in the production plane and at an angle ξ from the line of flight of the eta.

A three-body final state has five external degrees of freedom: three particles, each with three components of momentum, minus the four energy-momentum equations of constraint. One of these degrees of freedom, the orientation of the production plane in space (say, in the bubble chamber) is of no interest. Thus the four independent variables,

cos ξ, cos θ, ϕ, and the invariant mass-squared of the $\tilde{N}$, M^2, are sufficient to completely describe an event.

In terms of these independent variables, the differential cross section can be written

$$d^4\sigma = (\frac{1}{kE})|\mathcal{M}|^2(\frac{\rho}{E}\ dM^2\, d\cos\xi\, d\cos\theta\, d\phi), \qquad (5)$$

where the first factor is the Lorentz-invariant flux factor, the second is the absolute square of the matrix element, and the third is the Lorentz-invariant three-body phase-space factor. The factor ρ equals pq/M.

B. Mass and Angular Distributions

The production Dalitz plots and their mass-squared projections for our three sets of data are shown in Fig. 7. The distributions in the angular variables, $d\sigma/d\cos\xi$, $d\sigma/d\phi$, and $d\sigma/d\cos\theta$, are shown in Figs. 8, 9, and 10, respectively. All errors are statistical and are based only upon the number of events in each bin. The curves shown are the result of the best fit of the parameterization described in Section V.

In Fig. 7 we see that the events are clustered into the upper left-hand corners of the Dalitz plots as a result of the formation of the $\Delta(1238) \rightarrow \pi p$. It is seen that the enhancements in the low-mass region of the $M^2_{\eta p}$ distributions are a reflection of the Δ. The distributions in $M^2_{\eta\pi}$ (not shown) show no enhancements.

The distributions in cos ξ, Fig. 8, are the production angular distributions. Production via only s-wave would require these distributions to be completely flat. (We will use lower-case letters to indicate the

angular momentum state in which the eta and $\tilde{N}$ is produced, and capital letters to indicate the state in which the $\tilde{N}$ decays.) We see that the "flat" hypothesis is a good one at 1170 MeV/c (χ^2 = 3.8 for the π^+ data and 4.9 for the π^- data, with $\langle \chi^2 \rangle$ = 4.0), indicating that higher ℓ values may not be required.

However, the distributions in the azimuthal angle,[21] ϕ, which are shown in Fig. 9, indicate that p-wave production amplitudes are also required. The 1170-MeV/c π^+ data in particular show a very definite cos ϕ dependence. Production via only s-wave would require the ϕ distributions to be flat. As will become apparent in the next section, it is necessary to add p-wave production amplitudes in order to obtain a cos ϕ dependence.

The distributions in cos θ, Fig. 10, are the $\tilde{N}$ decay angular distributions. If the reaction proceeded solely via s-wave production of the $\Delta(1238)$, the distributions would be of the form $(1 + 3\cos^2\theta)$. If some p-wave Δ production were present, the distributions would no longer be of this form but would still be symmetrical. Asymmetry in the distributions is the result of both S-wave and P-wave decay of the $\tilde{N}$. The structure of these distributions is such as to be adequately described by only S- and P-wave decay of the $\tilde{N}$ (i.e., partial waves with $L > 1$ are not needed).

The qualitative remarks made in this section concerning the angular distributions are made more quantitative in the next section. On the basis of the distributions in cos ξ, cos θ, and ϕ, we consider only partial waves with ℓ = 0 and 1, and L = 0 and 1; that is, s- and p-wave production of the eta and $\tilde{N}$, and S- and P-wave decay of the $\tilde{N}$.

V. PARAMETERIZATION

If we list all possible final state amplitudes which can be produced with $\ell = 0$ and 1, and $L = 0$ and 1, we find a total of ten (see Appendix A). In addition, each complex amplitude, $(\ell\ L_J)_g$, can exist in two overall I-spin states: $I = 1/2$ and $I = 3/2$. We want to determine which amplitudes are required by the data and what are the values of the magnitudes and phases of these amplitudes. The $I = 3/2$ amplitudes can be determined from the π^+ data, as π^+p state exists only in $I = 3/2$. The π^-p state, however, consists of both $I = 3/2$ and $I = 1/2$. Once the $I = 3/2$ parameters have been determined from the π^+ data, this information can be used to determine the $I = 1/2$ parameters from the π^- data at the same momentum.

At first glance it may seem presumptuous to consider ten complex amplitudes with the order of only a hundred events. This would be true if all we had to work with was one angular distribution, as we certainly could not fit the distribution beyond a few powers in the cosine of the angle; and thus the number of amplitudes which could be determined would be severely limited. However, in our experiment we have four independent variables and therefore a total of four independent mass and angular distributions to work with, plus all the correlations which exist among the four variables. We do not fit beyond the second power in any one angular distribution. We will show that only four of the ten complex $I = 3/2$ amplitudes are required by the π^+ data and only one of the ten $I = 1/2$ amplitudes is required by the π^- data. Thus we have seven $I = 3/2$ parameters to be determined (four magnitudes and three phases) and two $I = 1/2$ parameters (one magnitude and one phase).

With four independent variables, and using the correlations which exist among the variables, we can determine seven parameters quite well with the order of only a hundred events.

We will now describe our technique for examining these correlations. We then go on to describe the procedure used to determine which of the ten complex amplitudes are present for each I-spin state and how the values of the magnitudes and phases of these amplitudes were determined. The results of this parameterization are then examined.

A. Method of Moments

For each I-spin state, the absolute square of the matrix element, $|\mathcal{M}|^2$, composed of the ten complex amplitudes, is derived as in Appendix A and has the form

$$|\mathcal{M}|^2 = \sum_{i=1}^{14} C_i(M_{\pi p}^2)\frac{1}{2}[y_\ell^m(\xi,0)Y_L^{-M}(\theta,\phi) + y_\ell^{-m}(\xi,0)Y_L^M(\theta,\phi)]$$

$$= C_1 y_0^0 Y_0^0 + C_2 y_1^0 Y_0^0 + C_3 y_0^0 Y_1^0 + C_4 y_1^0 Y_1^0$$

$$+ C_5 \frac{1}{2}(y_1^1 Y_1^{-1} + y_1^{-1} Y_1^1) + C_6 y_2^0 Y_0^0 + C_7 y_0^0 Y_2^0$$

$$+ C_8 y_2^0 Y_1^0 + C_9 \frac{1}{2}(y_2^1 Y_1^{-1} + y_2^{-1} Y_1^1)$$

$$+ C_{10} y_1^0 Y_2^0 + C_{11} \frac{1}{2}(y_1^1 Y_2^{-1} + y_1^{-1} Y_2^1)$$

$$+ C_{12} y_2^0 Y_2^0 + C_{13} \frac{1}{2}(y_2^1 Y_2^{-1} + y_2^{-1} Y_2^1)$$

$$+ C_{14} \frac{1}{2}(y_2^2 Y_2^{-2} + y_2^{-2} Y_2^2), \qquad (6)$$

where the C's are real functions of $M^2_{\pi p}$ ($M^2_{\pi p} \equiv M^2$, one of our four independent variables) consisting of combinations of the ten complex amplitudes $(\ell\ L_J)_\vartheta$ (see Appendix A), and where $\mathcal{Y}^m_\ell(\xi, 0)$ and $Y^M_L(\theta, \phi)$ are the production and decay spherical harmonics, respectively. The quantities L, ℓ, and the angular variables are defined in Section IV, and $-\ell \leq m \leq \ell$, $-L \leq M \leq L$.

One possible method for determining which of the ten complex amplitudes are required by the data is to insert Eq. (6) into Eq. (5) and then integrate over three of the four variables to get expressions for the mass distribution and the three angular distributions in terms of the complex amplitudes. A fit to these distributions would then yield some information as to which amplitudes are present. This procedure, however, does not make use of all the information contained in the data, as the various correlations which exist among the four variables integrate out when one obtains a mass or angular distribution.

In order to take these correlations into account, we project out each of the 14 coefficients of the various combinations of the production and decay spherical harmonics present in $|\mathcal{M}|^2$. We make use of the orthonormal property of the spherical harmonics,

$$\int (\mathcal{Y}^m_\ell Y^M_L)^* (\mathcal{Y}^{m'}_\ell Y^{M'}_{L'})\, d\cos\xi\, d\cos\theta\, d\phi = \delta_{\ell\ell'}\delta_{mm'}\delta_{LL'}\delta_{MM'}.$$

Thus,

$$C_i(M^2_{\pi p}) = \int \gamma_m \left[\mathcal{Y}^m_\ell Y^{-M}_L + \mathcal{Y}^{-m}_\ell Y^M_L\right]^*_i d\cos\xi\, d\cos\theta\, d\phi, \qquad (7)$$

where $\gamma_m = 1/2$ when $m = M = 0$, and $\gamma_m = 1$ when $m = -M \neq 0$. We define the values

$$D_i \equiv \frac{1}{kE^2} \int dM^2 \rho\, C_i(M^2), \tag{8}$$

where $\rho = pq/M$ and, as defined before, k is the linear momentum of the beam pion and p is that of the eta in the overall center of mass; E is the total energy in that center of mass; q is the linear momentum of the decay proton in the $\tilde{N}$ rest frame; and M is the mass of the $\tilde{N}$.

We performed operations (7) and (8) on our three sets of data. That is, in each of the M^2 bins we added up the values of $\gamma_m(y_\ell^{m} Y_L^{-M} + y_\ell^{-m} Y_L^{M})$ to get the distribution

$$\rho\, C_i(M_j^2) = \sum_{\substack{\text{number}\\ \text{of events}\\ \text{in bin j}}} \gamma_m(y_\ell^{m} Y_L^{-M} + y_\ell^{-m} Y_L^{M})_{ij} .$$

The value of the error for each bin is given by

$$\delta[\rho\, C_i(M_j^2)] = \left\{ \sum_{\substack{\text{number}\\ \text{of events}\\ \text{in bin j}}} [\gamma_m(y_\ell^{m} Y_L^{-M} + y_\ell^{-m} Y_L^{M})_{ij}]^2 \right\}^{1/2} .$$

We then obtained the value D_i by summing over the M^2 bins and multiplying by a scale factor to convert from counts to cross section. Thus,

$$D_i = (\text{scale factor}) \sum_{j \text{ bins}} \rho\, C_i(M_j^2)$$

and

$$\delta D_i = (\text{scale factor}) \left\{ \sum_{\substack{\text{total}\\ \text{no. of}\\ \text{events}}} [\gamma_m(y_\ell^{m} Y_L^{-M} + y_\ell^{-m} Y_L^{M})_i]^2 \right\}^{1/2} .$$

The 14 D values for each of the three sets of data are presented in Table III.

As stated at the beginning of this subsection, each mass dependent coefficient $C_i(M^2)$ consists of combinations of the mass-dependent parts of all the complex amplitudes. The type of amplitudes present in each $C_i(M^2)$, and hence in each D_i, is given in Table IV. (This table is derived in Appendix A.) In the following subsections, by comparing Tables III and IV, we obtain the simplest set of amplitudes necessary to fit the data.

B. The π^+ Data

1. Determination of the I = 3/2 amplitudes

From the Dalitz plots and angular distributions we believe that the $\Delta(1238)$ is produced. We therefore need at least one amplitude representing Δ production. Of the ten I = 3/2 amplitudes, $(\ell L_J)_J$, under consideration, four of them, $(sP_{3/2})_{3/2}$, $(pP_{3/2})_{1/2, 3/2, 5/2}$, represent the production of the Δ. [When states differ only in the total angular momentum J we use the notation $(\ell L_J)_{J_1, J_2, \cdots}$.] We begin by choosing the lowest orbital angular momentum state amplitude $(sP_{3/2})_{3/2}$. Next we see from the π^+ part of Table III (columns 1a and 2a) that D_3, D_5, D_7 (and of course D_1, since $D_1 = \sigma$) are nonzero. We see from Table IV that in order to make D_3 nonzero we need sS-sP and/or pS-pP interference. (The values of J and J have been suppressed.) To obtain sS-sP interference we need only to assume one additional amplitude, $(sS_{1/2})_{1/2}$. However, in order to obtain pS-pP interference there are seven additional amplitudes which need to be considered, all of which possess higher angular momentum barriers than the sS amplitude. On the basis of always choosing the lowest

angular momentum state amplitudes, we choose the former alternative.

In order to make D_5 nonzero we see from Table IV that we have to add either pS or pP amplitudes. Again choosing the amplitudes with the lower angular momentum barriers, we add the pS amplitudes to our set. The $(pS_{1/2})_{1/2}$ final state originates from the $\mathcal{S}_{1/2}$ initial state, the $(pS_{1/2})_{3/2}$ final state from the $\mathcal{D}_{3/2}$ initial state. Because the momentum of the beam particle in the overall center of mass is of the order of 600 MeV/c, there is sufficient energy for the initial state to exist in $\mathcal{D}$-wave. We therefore include both the $(pS_{1/2})_{1/2}$ and $(pS_{1/2})_{3/2}$ amplitudes.

Next we see from Table IV that in order for D_7 to be nonzero, we need sP-sP and/or pP-pP interference. As we have already chosen the $(sP_{3/2})_{3/2}$ amplitude, no additional amplitudes are required.

Thus in order to obtain nonzero values of D_1, D_3, D_5, and D_7 we need only the amplitudes: $(sS_{1/2})_{1/2}$, $(sP_{3/2})_{3/2}$, and $(pS_{1/2})_{1/2,3/2}$. We assume all other amplitudes are absent. This means that when the $\tilde{N}$ is in S-wave, we have both s- and p-wave production; when the $\tilde{N}$ is in P-wave, it has only J-3/2, and is produced only in s-wave.

With this choice of amplitudes, all shaded portions of Tables III, IV, and AII should be zero. We see that our assumption that the five (pP) amplitudes are zero requires D_8 through D_{14} to be zero. Except for the 1050-MeV/c value of D_8, this requirement is consistent with the D values of Table III. The nonzero value at 1050 MeV/c could be a statistical fluctuation.

2. Determination of the values of the magnitudes and phases of the complex amplitudes

Now that we have described the procedure used to determine which complex amplitudes are present in the π^+ data, we describe how the magnitudes and phases of these amplitudes were determined. Near threshold the M^2 and E dependence of the amplitude for $\mathcal{L}_\mathcal{J} \to (\ell\ L_J)_\mathcal{J}$ can be parameterized by $A_{\alpha\beta}\ e^{i\lambda_{\alpha\beta}}\ k^{\mathcal{L}}\ p^{\ell}\ q^{L}$, where the quantities $A_{\alpha\beta}$ are real positive parameters (assumed to be energy independent), $\lambda_{\alpha\beta}$ are phase angles (also assumed to be energy independent), and α and β are indices used to differentiate the various states ($\alpha = 0$ for s-wave and $2\mathcal{J}$ for p-wave; similarly $\beta = 0$ for S-wave and 2J for p-wave). Specifically, for our set of four amplitudes, we have

$\mathcal{L}_\mathcal{J} \to (\ell\ L_J)_\mathcal{J}$	M^2 and E dependence
$\mathcal{P}_{1/2} \to (sS_{1/2})_{1/2}$	$A_{00}\ e^{i\lambda_{00}}\ k$
$\mathcal{D}_{3/2} \to (sP_{3/2})_{3/2}$	$A_{03}\ e^{i\lambda_{03}}\ k^2\ (M/q\Gamma)^{1/2}\ [1/(\epsilon-i)]$
$\mathcal{S}_{1/2} \to (pS_{1/2})_{1/2}$	$A_{10}\ e^{i\lambda_{10}}\ p$
$\mathcal{D}_{3/2} \to (pS_{1/2})_{3/2}$	$A_{30}\ e^{i\lambda_{30}}\ p\ k^2$

where the factor, $(M/q\Gamma)^{1/2}\ [1/(\epsilon-i)]$ is the Breit-Wigner amplitude for the $\Delta(1238)$ resonance.[22] The factor ϵ is the number of half widths removed from the resonant energy. That is,

$$\epsilon = \frac{M_0^2 - M^2}{M_0\Gamma} \approx \frac{M_0 - M}{\Gamma/2},$$

where[23]

$$\Gamma = \Gamma_0 \left(\frac{q}{q_0}\right)^3 \left\{\frac{[(M+m_p)^2 - m_\pi^2]/M^2}{[(M_0+m_p)^2 - m_\pi^2]/M_0^2}\right\},$$

with (Ref. 13) $M_0 = 1236$ MeV, $\Gamma_0 = 120$ MeV; and $q_0 = 231$ MeV. Because there is an overall arbitrary phase, we define $\lambda_{03} \equiv 0$. We further define $F \equiv (M/q\Gamma)[1/(\epsilon^2+1)]$ and $G \equiv (q\Gamma/M)^{1/2}$. Inserting these definitions into the expressions for the C's as derived in Appendix A, and using the above table, we obtain for the I = 3/2 amplitudes:

$$\begin{aligned}
C_1(M^2) &= [A_{00}^2 k^2] + [2A_{03}^2 k^4]F + [A_{10}^2 + 2A_{30}^2]p^2, \\
C_2(M^2) &= [\tfrac{2}{\sqrt{3}} A_{00} A_{10} k \cos(\lambda_{00}-\lambda_{10}) + \tfrac{4}{\sqrt{3}} A_{00} A_{30} k^3 \cos(\lambda_{00}-\lambda_{30})]p, \\
C_3(M^2) &= [\tfrac{4}{\sqrt{3}} A_{00} A_{03} k^3 \cos\lambda_{00}]GF\epsilon + [\tfrac{4}{\sqrt{3}} A_{00} A_{03} k^3 \sin\lambda_{00}]GF, \\
C_4(M^2) &= [\tfrac{4}{3} A_{10} A_{03} k^2 \cos\lambda_{10} + \tfrac{8}{3} A_{30} A_{03} k^4 \cos\lambda_{30}]pGF\epsilon \\
&\quad + [\tfrac{4}{3} A_{10} A_{03} k^2 \sin\lambda_{10} + \tfrac{8}{3} A_{30} A_{03} k^4 \sin\lambda_{30}]pGF, \qquad (9) \\
C_5(M^2) &= [\tfrac{4}{3} A_{10} A_{03} k^2 \cos\lambda_{10} - \tfrac{4}{3} A_{30} A_{03} k^4 \cos\lambda_{30}]pGF\epsilon \\
&\quad + [\tfrac{4}{3} A_{10} A_{03} k^2 \sin\lambda_{10} - \tfrac{4}{3} A_{30} A_{03} k^4 \sin\lambda_{30}]pGF, \\
C_6(M^2) &= [\tfrac{4}{5^{1/2}} A_{10} A_{30} k^2 \cos(\lambda_{10}-\lambda_{30}) + \tfrac{2}{5^{1/2}} A_{30}^2 k^4]p^2, \\
C_7(M^2) &= [\tfrac{2}{5^{1/2}} A_{03}^2 k^4]F,
\end{aligned}$$

$$D_i = \frac{1}{kE^2} \int C_i(M^2)\rho \, dM^2. \qquad (8)$$

The A's and λ's were determined by fitting the 1050- and 1170-MeV/c π^+ data. Equating the numerical value of each D_i as given in Table III with the algebraic expression for the D_i as given by Eqs. (8) and (9), we obtain a set of seven quadratic equations involving the four

A's and three λ's. For example,

$$D_1 = A_{00}^2\left[\frac{k}{E^2}\int \rho\, dM^2\right] + 2A_{03}^2\left[\frac{k^3}{E^2}\int \rho\, F\, dM^2\right]$$
$$+ (A_{10}^2 + 2A_{30}^2 k^4)\left[\frac{1}{kE}\int \rho\, p^2\, dM^2\right], \qquad (10)$$

which at 1170 MeV/c becomes

$$(53.3 \pm 5.0)\mu b = A_{00}^2[1.58\times 10^{-3}\ \text{BeV}^2] + 2A_{03}^2[7.49\times 10^{-3}\ \text{BeV}^3]$$
$$+ A_{10}^2[1.88\times 10^{-4}\ \text{BeV}^2] + 2A_{30}^2[2.83\times 10^{-5}\ \text{BeV}^6].$$

The integrations have been performed numerically. At each momentum we have seven such equations. In addition, $C_1(M^2)$, $C_3(M^2)$, $C_4(M^2)$, and $C_5(M^2)$ each have two or more final state momentum dependences; therefore, the relative amounts of each dependence can be fit, thereby yielding more information on the values of the parameters. [The distributions $C_2(M^2)$, $C_6(M^2)$, and $C_7(M^2)$ each have only one momentum dependence and therefore yield no additional information on the values of the A's and λ's.] We fitted $C_1(M^2)$, $C_3(M^2)$, $C_4(M^2)$, and $C_5(M^2)$ and the seven D_i's at both π^+ momenta simultaneously and obtained the fitted values[24]

$$A_{00} = (66^{+9}_{-13})[\mu b/\text{BeV}^2]^{1/2} \qquad \lambda_{00} = (4.83^{+0.08}_{-0.14})\ \text{rad},$$
$$A_{10} = (166^{+19}_{-21})[\mu b/\text{BeV}^2]^{1/2} \qquad \lambda_{10} = (4.39^{+0.44}_{-0.37})\ \text{rad},$$
$$A_{30} = (221^{+21}_{-17})[\mu b/\text{BeV}^6]^{1/2} \qquad \lambda_{30} = (0.67^{+0.20}_{-0.41})\ \text{rad},$$
$$A_{03} = (51.7^{+3.0}_{-3.7})[\mu b/\text{BeV}^3]^{1/2}, \qquad (11)$$

with $\chi^2 = 88$, $\langle \chi^2 \rangle = 71$.

3. Comparison at the π^+ data with the results of the fit

With knowledge of the A's and λ's, by Eqs. (8) and (9), we should be able to predict the distributions of all seven $C_i(M^2)$ and the values of the seven D_i's, and hence the mass and angular distributions and the total cross section for the reaction $\pi^+ p \to \pi^+ p\eta$ at any momentum near threshold.

Figure 5 shows the variation in cross section with beam momentum. The curve labeled "u=0" is the cross section as given by the values at the parameters, Eq. (11). We see that the curve follows the data well from threshold to just above 1170 MeV/c, whereupon it continues to rise steadily, departing from the data. (The other curves will be discussed in the following subsections.)

For the angular distributions the differential cross sections are obtained by integrating Eq. (5) with respect to the appropriate variables. Thus,

$$\frac{d\sigma}{d\cos\xi} = \left[(D_1 - \frac{5^{1/2}}{2} D_6) + (\sqrt{3}\, D_2)\cos\xi + (\frac{3}{2} 5^{1/2} D_6)\cos^2\xi \right] / [\text{no. of bins}], \tag{12}$$

$$\frac{d\sigma}{d\phi} = \left[D_1 + (\frac{-3\pi^2}{32} D_5)\cos\phi \right] / [\text{no. of bins}], \tag{13}$$

$$\frac{d\sigma}{d\cos\theta} = \left[(D_1 - \frac{5^{1/2}}{2} D_7) + (\sqrt{3}\, D_3)\cos\theta + (\frac{3}{2} 5^{1/2} D_7)\cos^2\theta \right] / [\text{no. of bins}]. \tag{14}$$

The values of the seven D_i's at 1050 and 1170 MeV/c, as given by the values of the parameters, Eq. (11), are listed in Table III beside the experimental values. The curves shown in the angular distributions, Figs. 8, 9, and 10, are obtained by using the fitted D_i's in Eqs. (12),

(13), and (14), respectively. It is seen that the curves follow the data quite well.

The mass distributions $d\sigma/dM^2_{\pi p}$ and $d\sigma/dM^2_{\eta p}$ can be obtained by integrating the expression

$$d^2\sigma = \frac{1}{kE^2} \frac{dM^2_{\pi p}\, dM^2_{\eta p}}{4E} \left| \mathcal{M}\,(M^2_{\pi p},\ M^2_{\eta p}) \right|^2,$$

which is a differential element of the Dalitz plot, with respect to the appropriate variable. Thus,

$$\frac{d\sigma}{dM^2_{\pi p}} = \frac{1}{kE^2}\, \rho\, C_1(M^2_{\pi p}), \tag{15}$$

$$\frac{d\sigma}{dM^2_{\eta p}} = \frac{1}{4kE^3} \int_{\min(M^2_{\eta p})}^{\max(M^2_{\eta p})} C_1(M^2_{\pi p})\, dM^2_{\pi p}\,. \tag{16}$$

These parameterized curves are shown in Fig. 7.

From Eq. (10) we see that D_1 consists of the sum of the intensities of the four I = 3/2 amplitudes and is therefore the sum of four partial cross sections.[25] These partial cross sections are listed in Table V. We see that the $\Delta(1238)$ accounts for more than half of the reaction at 1050 MeV/c and about three-fourths of the reaction at 1170 MeV/c, with the rest accounted for by nonresonant three-body states in which the eta is produced in both s-wave and p-wave with the (π-p) system in a relative S-state.

C. Other Experiments Involving the Reaction $\pi^+ p \to \pi^+ p\eta$

We found in the preceding subsection that the cross section, as given by the parameters of Eq. (11), rises steeply beyond 1170 MeV/c, departing from the data. In an attempt to get a parameterized cross section which better follows the data above 1170 MeV/c, we introduce an energy dependence into the quantities $A_{\alpha\beta}$. We replace $A_{\alpha\beta}$ with $A_{\alpha\beta}/[1 + (u/\pi)^{1/2} f_{\alpha\beta}(E)]$, where $f_{\alpha\beta}(E)$ is a function of energy such that at threshold $f_{\alpha\beta}(E) = 0$. The function $f_{\alpha\beta}(E)$ is chosen such that at high energy it cancels the threshold kinematical factors; hence, $\sigma_{\alpha\beta} \xrightarrow[k\to\infty]{} (1/u)(\vartheta_{\alpha\beta} + \frac{1}{2})\pi/k^2$, which is 1/u times the unitarity limit for that partial wave. Thus, we choose $f_{\alpha\beta} = n_{\alpha\beta}(A_{\alpha\beta}/E) \times (k^{2\mathcal{L}+1} p_M^{2\ell+1} q^{2L+1} Q)^{1/2}$ for the nonresonant amplitudes, and $f_{\alpha\beta} = n_{\alpha\beta}(A_{\alpha\beta}/E)(k^{2\mathcal{L}+1} p_M^{2\ell+1} Q)^{1/2}$ for the resonant amplitude, where p_M and q_M are the maximum values of p and q, respectively, at energy E and $Q = E - m_\eta - m_\pi - m_p$. The constant $n_{\alpha\beta}$ is chosen such that at high energy, $[(A_{\alpha\beta}^2/E^2)\, k^{2\mathcal{L}+1} \int \rho\, p^{2\ell}\, g\, dM^2]/[f_{\alpha\beta}(E)]^2 = 1$, where $g = F$, the Breit-Wigner intensity, for the resonant amplitude, and $g = 1$ for the nonresonant amplitude. For simplicity we take the dimensionless parameter u to be the same for all four amplitudes. Since $u = 1$ for the unitarity limit, we must have $u \geq 1$ for nonviolation of unitarity.

Fitting only our 1050- and 1170-MeV/c data to this hypothesis, we obtain,

$$A_{00} = (71^{+27}_{-25})\ [\mu b/BeV^2]^{1/2} \qquad \lambda_{00} = (4.89^{+0.28}_{-0.37})\ \text{rad},$$

$$A_{10} = (212^{+74}_{-62})\ [\mu b/BeV^2]^{1/2} \qquad \lambda_{10} = (4.36^{+0.21}_{-0.28})\ \text{rad},$$

$$A_{30} = (329^{+87}_{-90})\ [\mu b/BeV^6]^{1/2} \qquad \lambda_{30} = (0.61^{+0.23}_{-0.38})\ \text{rad},$$

$$A_{03} = (296^{+80}_{-35})\ [\mu b/BeV^3]^{1/2},$$

$$u = (94^{+17}_{-32}), \tag{17}$$

with $\chi^2 = 80$, $\langle \chi^2 \rangle = 70$.

Figure 5 displays the cross-section curve resulting from the parameters of Eq. (17). We see that our best fit value, u = 94, gives a predicted cross section that lies below the ten measured cross sections located between 1.2 and 3.7 BeV/c. (The overall χ^2 is 80 + 25, with $\langle \chi^2 \rangle$ = 70 + 10.) By decreasing u to 67, we decrease the overall χ^2 to (81 + 15) = 96, where the contribution from our data alone is 81. This is in good agreement with $\langle \chi^2 \rangle = 80 \pm (2\langle \chi^2 \rangle)^{1/2} = 80 \pm 13$. Thus our simple model for the energy dependence of the parameters, $A_{\alpha\beta}$, involving just one additional parameter, u, gives good agreement with all of our data and with the ten additional cross sections lying between 1.2 and 3.7 BeV/c. However, in order for the parameter values to be meaningful, we must be able to predict not only the value of the total cross section at a particular beam momentum, but also all the mass and angular distributions at that momentum.

The published distributions of Refs. 2-7 are reproduced in Fig. 11; the curves are those predicted by the parameters which produce the u = 67 curve of Fig. 5. It is seen that all mass distributions are in good agreement. The production angular distributions are in good agreement at low energy, but our fit is unable to produce the forward

peaking that arises with increased beam momentum. The only decay angular distributions which are available are those of Ref. 2, and they are not well represented by the curves. Thus, the assumption of phases which are constant with beam momentum probably becomes inadequate, and/or more partial waves become necessary at these higher energies.

D. The π^- Data

While the $\pi^+ p$ state consists of only I = 3/2 amplitudes, the $\pi^- p$ state has both I = 3/2 and I = 1/2 amplitudes. Thus, for the $\pi^- p$ reaction each complex amplitude $(\ell\ L_J)_\vartheta$ becomes

$$(\ell\ L_J)_\vartheta \rightarrow \tfrac{1}{3}(\ell\ L_J)_\vartheta^{I=1/2} + \tfrac{2}{3}(\ell\ L_J)_\vartheta^{I=3/2}, \tag{18}$$

and therefore,

$$\begin{aligned}[(\ell\ L_J)_\vartheta\ ][(\ell'\ L'_{J'})_{\vartheta'}]^* \rightarrow\ & \tfrac{1}{9}[(\ell\ L_J)_\vartheta^{I=3/2}][(\ell'\ L'_{J'})_{\vartheta'}^{I=3/2}]^* \\ & + \tfrac{2}{9}[(\ell\ L_J)_\vartheta^{I=3/2}][(\ell'\ L'_{J'})_{\vartheta'}^{I=1/2}]^* \\ & + \tfrac{2}{9}[(\ell\ L_J)_\vartheta^{I=1/2}][(\ell'\ L'_{J'})_{\vartheta'}^{I=3/2}]^* \\ & + \tfrac{4}{9}[(\ell\ L_J)_\vartheta^{I=1/2}][(\ell'\ L'_{J'})_{\vartheta'}^{I=1/2}]^* .\end{aligned}$$

We see that if all the I = 1/2 amplitudes were zero, then each $C_i(M^2)$ for the π^- data would be 1/9 of the corresponding $C_i(M^2)$ for the π^+ data (at the same momentum). Of course the same relationship would hold for each D_i.

From Table III we see that at 1170 MeV/c, $D_1(\pi^-)$ is not equal to 1/9 of $D_1(\pi^+)$; i.e., the ratio of the total cross sections is not 1/9. Therefore at least one I = 1/2 amplitude is required. We also see that,

like the π^+ data, each $D_i(\pi^-)$, i = 8 to 14, is consistent with zero so that there is no need to consider I = 1/2 pP amplitudes. Next we see from Table IV that if the I = 1/2 $(sS_{1/2})_{1/2}$ amplitude is present, we expect it to contribute to $D_2(\pi^-)$ through sS-pS interference (where the pS amplitude exists in I = 3/2) and to $D_3(\pi^-)$ through sS-sP interference (where the sP amplitude exists in I = 3/2). Therefore if the I = 1/2 $(sS_{1/2})_{1/2}$ amplitude contributes, $D_1(\pi^-)$, $D_2(\pi^-)$, and $D_3(\pi^-)$ are not constrained to be 1/9 of their corresponding π^+ values. Similarly, from Table IV we see that if a I = 1/2 (pS) amplitude is present, then $D_1(\pi^-)$, $D_2(\pi^-)$, $D_4(\pi^-)$, $D_5(\pi^-)$, and $D_6(\pi^-)$ are not constrained to be 1/9 of their corresponding π^+ values. Finally, if an I = 1/2 (sP) amplitude is present, then $D_1(\pi^-)$, $D_3(\pi^-)$, $D_4(\pi^-)$, $D_5(\pi^-)$, and $D_7(\pi^-)$ are not constrained to the 1/9 value. Examination of Table III shows that, except for D_1, each experimental value $D_i(\pi^-)$ (column 3a) is consistent with 1/9 of the corresponding experimental value $D_i(\pi^+)$ (column 2a); the errors involved, however, are so large as to make the values insensitive to any inconsistencies with the 1/9 value. Thus, other than the fact that at least one I = 1/2 amplitude is required, comparison of the experimental π^- values with the experimental π^+ values (comparison of column 3a with column 2a of Table I) leads to no new information as to which I = 1/2 amplitudes are needed.

However, if we now make use of the values of the I = 3/2 amplitudes as determined by our fit to the π^+ data, we can compare the $D_i(\pi^-)$ values (column 3a) with the $D_i(\pi^+)$ values of column 2b. If this is done, we see that $D_2(\pi^-) = 2.90 \pm 1.63$ is almost two standard deviations away from 1/9 of $D_2(\pi^+) = 0.13$, indicating (from Table IV) that sS and/or pS I = 1/2 amplitudes may be present.

Considering the three I = 1/2 complex amplitudes, $(sS_{1/2})_{1/2}$, $(pS_{1/2})_{1/2,\,3/2}$, we proceeded, as we did with the π^+ data, to determine the magnitudes and phases (or the real and imaginary parts) of these amplitudes. Each $C_i(M^2)$ of Eq. (12) was modified to include the I = 1/2 parameters. As prescribed by Eq. (18),

$$A_{\alpha\beta}\, e^{i\lambda_{\alpha\beta}} \rightarrow \frac{1}{3} A_{\alpha\beta}\, e^{i\lambda_{\alpha\beta}} + \frac{2}{3} B_{\alpha\beta}\, e^{i\nu_{\alpha\beta}}, \qquad \alpha\beta = 00,\ 10,\ 30,$$

and

$$A_{\alpha\beta}\, e^{i\lambda_{\alpha\beta}} \rightarrow \frac{1}{3} A_{\alpha\beta}\, e^{i\lambda_{\alpha\beta}}, \qquad \alpha\beta = 03,$$

where the B's and the ν's are the magnitudes and phases, respectively, of the I = 1/2 complex amplitudes. Using these modified $C_i(M^2)$ and D_i expressions and using the A's and λ's of Eq. (11), we fitted the π^- data in the same manner as we had fitted the π^+ data, and obtained,

$$\mathrm{Re}\{B_{00}\, e^{i\nu_{00}}\} = (38\,^{+10}_{-17})\ [\mu b/\mathrm{BeV}^2]^{1/2},$$

$$\mathrm{Im}\{B_{00}\, e^{i\nu_{00}}\} = (-85\,^{+10}_{-9})\ [\mu b/\mathrm{BeV}^2]^{1/2},$$

$$\mathrm{Re}\{B_{10}\, e^{i\nu_{10}}\} = (-68\,^{+80}_{-113})\ [\mu b/\mathrm{BeV}^2]^{1/2},$$

$$\mathrm{Im}\{B_{10}\, e^{i\nu_{10}}\} = (77\,^{+71}_{-99})\ [\mu b/\mathrm{BeV}^2]^{1/2},$$

$$\mathrm{Re}\{B_{30}\, e^{i\nu_{30}}\} = (151\,^{+147}_{-140})\ [\mu b/\mathrm{BeV}^6]^{1/2},$$

$$\mathrm{Im}\{B_{30}\, e^{i\nu_{30}}\} = (-136\,^{+262}_{-158})\ [\mu\ /\mathrm{BeV}^6]^{1/2},$$

with $\chi^2 = 34$ and $\langle \chi^2 \rangle = 33$.

We see that B_{10} and B_{30} are consistent with zero and that therefore $(sS_{1/2})_{1/2}$ is the only I = 1/2 amplitude needed to fit the data. [Had we limited ourselves at the beginning of this subsection to only one I = 1/2 amplitude, the simplest hypothesis would have been

$(sS_{1/2})_{1/2}$; all other amplitudes are suppressed owing to angular momentum barriers with no strong forces acting, such as in the $\Delta(1238)$, to enhance any of them.] Setting $B_{10} \equiv 0$ and $B_{30} \equiv 0$ we obtain[24]

$$B_{00} = (93^{+11}_{-13})\ [\mu b/BeV^2]^{1/2} \qquad \nu_{00} = (5.12^{+0.11}_{-0.17})\ \text{rad},$$

with $\chi^2 = 37$, $\langle \chi^2 \rangle = 37$.

The $D_i(\pi^-)$ values as given by the fit are given in column 3b of Table III. The $D_i(\pi^-)$, i = 4 to 7, are of course 1/9 of the corresponding $D_i(\pi^+)$ value, as given by the π^+ fit, as B_{00} and ν_{00} do not enter into the expressions for these D's. The π^- angular distributions are shown in Figs. 8, 9, and 10; the curves are the distributions as given by Eqs. (12), (13), and (14), using these fitted $D_i(\pi^-)$ values. Agreement is good.

Because the $(sP_{3/2})_{3/2}$ and $(pS_{1/2})_{1/2,\,3/2}$ amplitudes are assumed to be present only in the I = 3/2 state, their relative contribution to the π^-p reaction can be computed as follows:

$$\left[\begin{array}{l}\text{relative}\\ \text{contribution}\\ \text{to } \pi^-p \text{ reaction}\end{array}\right] \sigma(\pi^-p \to \pi^-p\eta) = \frac{1}{9}\left[\begin{array}{l}\text{relative}\\ \text{contribution}\\ \text{to } \pi^+p \text{ reaction}\end{array}\right] \sigma(\pi^+p \to \pi^+p\eta).$$

Thus, as the reaction $\pi^+p \to \eta\Delta(1238)$ accounts for 73% of eta production in the π^+p reaction at 1170 MeV/c, the reaction $\pi^-p \to \eta\Delta(1238)$ accounts for (1/9) (73%) (53.3 μb/15.9 μb) = 27% of eta production in the π^-p reaction at this momentum. Similarly, 6% of the π^-p reaction proceeds via I = 3/2 (pS) amplitudes. The remainder of the reaction, 67%, is accounted for by the <u>total</u> sS intensity, which is composed of both I = 3/2 and I = 1/2 amplitudes. We cannot say how much of the reaction proceeds

via the I = 1/2 sS amplitude alone or via the I = 3/2 sS amplitude alone, as in any expression involving these two amplitudes, there is always present an interference term between them.[25] This interference term is present in $C_1(M^2)$, and hence in $d\sigma/dM^2_{\pi p}$ and in $d\sigma/dM^2_{\eta p}$. Thus, only the total sS contribution can be given. The relative contributions and the partial cross sections for the $\pi^- p$ reaction at 1170 MeV/c are listed in Table V.

The distributions in $M^2_{\pi p}$ and $M^2_{\eta p}$, as given by the values of the π^- parameters, are shown in Fig. 5. Again, agreement is good.

If we extrapolate the π^- parameters, assuming phases which are constant with beam momentum and an amplitude dependence as prescribed in Section VC with u = 67, we obtain the dashed curve of Fig. 5. The curve is in good agreement with the π^- cross-section points.

There are no mass or angular distributions published for points h^8 and i^9. For points j^{10} there are mass distributions which indicate that the $N^*(1688)$ and the $A_2(1300)$ are produced in addition to the $\Delta(1238)$. Thus more amplitudes are necessary at high energy.

E. The $N^*(1550) \rightarrow \eta p$ Resonance

In the last few years the existence of a resonance, the $N^*(1550)$, which decays mainly into ηp, has been inferred on the basis of phase shift analysis of $\pi^- p$ elastic scattering[26] and on the basis of experiments which exhibit a cross-section enhancement near threshold in the reactions $\gamma p \rightarrow \eta n$ and $\pi^- p \rightarrow \eta n$.[27] There has been one experiment reported in which the resonance has been seen as an enhancement in the η-N mass distribution in a reaction involving the final state of three or more particles.[28]

We see from our Dalitz plots in Fig. 7 that the mass and width values of the $N^*(1550)$ are such as to fill up the entire region of the plots; thus it is difficult to deduce the presence or absence of this resonance in our experiment. In order to make use of all four independent variables and all the correlations which exist among the variables, we have added amplitudes for the production of the $N^*(1550)$ resonance to the matrix element. (See Appendix B.) The $C_i(M^2_{\pi p})$ expressions derived in Appendix A are now replaced by more complicated expressions, $C_i(M^2_{\pi p}, M^2_{\eta p})$, and these new expressions are used to fit the data.

For the π^+ data we included in the fit I = 3/2 amplitudes for s-wave and p-wave production of the $N^*(1550)$ along with the original four I = 3/2 amplitudes of Section VB. At 1050 MeV/c, addition of the $N^*(1550)$ amplitudes does not change the chi-square minimum from that obtained with just the original four amplitudes. At 1170 MeV/c, we find a chi-square minimum at Re {s-wave amplitude} = (-4^{+7}_{-13}) $[\mu b/BeV]^{1/2}$, Im {s-wave amplitude} = (-8^{+8}_{-15}) $[\mu b/BeV]^{1/2}$, and p-wave amplitudes equal zero, with $\chi^2 = 41.0$, $\langle \chi^2 \rangle = 38$; setting both s-wave and p-wave $N^*(1550)$ amplitudes equal to zero, we obtain $\chi^2 = 42.3$, $\langle \chi^2 \rangle = 40$. Thus, production of the $N^*(1550) \rightarrow \eta p$ is undetectable in our π^+ data.

In fitting the π^- data, we set the I = 3/2 amplitudes for $N^*(1550)$ production equal to zero, because the π^+ data show that none are required. We find a χ^2 minimum at Re {s-wave amplitude} = (1.1 ± 2.1) $[\mu b/BeV]^{1/2}$, Im {s-wave amplitude} = (0.3 ± 1.7) $[\mu b/BeV]^{1/2}$, and p-wave amplitudes equal zero, with $\chi^2 = 37.7$, $\langle \chi^2 \rangle = 43$; setting both s- and p-wave $N^*(1550)$ amplitudes equal to zero, we obtain $\chi^2 = 37.8$,

$\langle \chi^2 \rangle = 45$. Thus, the decay $N^*(1550) \rightarrow \eta p$ is undetectable in our π^- data.

We next ask, what are the upper limits for the reaction $\pi^\pm p \rightarrow \pi^\pm N^*(1550);\ N^*(1550) \rightarrow \eta p$? When the matrix element contains amplitudes for $N^*(1550)$ production, the cross section is not composed of the sum of the partial cross sections due to each amplitude. There are always present interference terms involving the $N^*(1550)$.[25] Thus, in obtaining an upper limit, we cannot quote a cross section due to the $N^*(1550)$ alone. If, however, we attribute all interference terms involving the $N^*(1550)$, as well as the $N^*(1550)$ intensity terms, to the formation of the resonance, we obtain at the 90% confidence level,

$$\frac{\sigma[\pi^+ p \rightarrow \pi^+ N^*(1550);\ N^*(1550) \rightarrow \eta p]}{\sigma(\pi^+ p \rightarrow \pi^+ p\eta)} \leq 0.08 \ (0.8\ \mu b) \text{ at } 1050 \text{ MeV/c},$$

$$\leq 0.19 \ (10.1\ \mu b) \text{ at } 1170 \text{ MeV/c}.$$

Assuming the $I = 3/2$ amplitudes for $N^*(1550)$ production are zero at 1170 MeV/c, we obtain at the 90% confidence level an upper limit on $I = 1/2$ $N^*(1550)$ amplitudes of 7.6 μb, or

$$\frac{\sigma[\pi^- p \rightarrow \pi^- N^*(1550);\ N^*(1550) \rightarrow \eta p]}{\sigma(\pi^- p \rightarrow \pi^- p\eta)} \leq 0.48.$$

VI. SUMMARY

A simple phenomenological model has been presented which describes eta production in the reaction $\pi p \rightarrow \pi p \eta$ near threshold. From a partial wave analysis, using our π^+ data at 1050 and 1170 MeV/c and π^- data at 1170 MeV/c, we found that four I = 3/2 amplitudes, $(sS_{1/2})_{1/2}$, $(sP_{3/2})_{3/2}$, and $(pS_{1/2})_{1/2,\,3/2}$, are required by the π^+ data and that an additional I = 1/2 amplitude, $(sS_{1/2})_{1/2}$, is required by the π^- data. The magnitudes and phases of these amplitudes have been determined.

We found that the $\pi^+ p$ reaction is dominated by s-wave production of the $\Delta(1238) \rightarrow \pi^+ p$ resonance, while the $\pi^- p$ reaction is dominated by the I = 1/2 amplitude in which all particles are in relative S-states. The fitted parameters produce a cross section variation with energy, and mass and angular distributions which are in good agreement with our data.

The parameters were then extrapolated to higher energies where we obtained good agreement with the energy variation of the cross section and with some of the published mass and angular distributions. It appears, however, that as the beam momentum increases, an energy variation of the phases and/or more partial waves probably become necessary.

We further find that the reaction $\pi p \rightarrow \pi N^*(1550)$, $N^*(1550) \rightarrow \eta p$ is undetectable in both our π^+ and π^- data; upper limits are obtained.

ACKNOWLEDGMENTS

It is a pleasure to acknowledge the continued interest and support of Professor Luis W. Alvarez. In addition we are grateful to Dr. Earle C. Fowler and to L. J. Lloyd for their contributions to the data analysis.

APPENDICES

A. Derivation of the Matrix Element

We want to derive the absolute square of the matrix element, Eq. (6), arising from the ten complex amplitudes considered in Section V. The ten amplitudes written in terms of $\mathcal{L}_{\mathcal{J}} \rightarrow (\ell\ L_J)_{\mathcal{J}}$ are listed in Table AI. (See Section IV for notation.)

We take the beam direction as the quantization axis. (See Section IV.) Along this axis the initial π-p state has $\mathcal{J}_z = \pm\frac{1}{2}$, the spin projection of the proton, as there can be no component of the initial orbital angular momentum $\mathcal{L}$ along the beam. We expand the states $(\ell\ L_J)_{\mathcal{J}}$ in terms of spherical harmonics. In general,

$$
\begin{aligned}
(\ell\ L_J)_{\mathcal{J}} &= a(M^2_{\pi p})\,|\,\ell\ LJ,\ \mathcal{J}\mathcal{J}_z\rangle \\
&= a(M^2_{\pi p}) \sum_{m=\ \mathcal{J}_z - M_J} \langle \ell m;\ JM_J|\ \mathcal{J}\mathcal{J}_z\rangle\,|\ell m\rangle\,|JM_J\rangle \\
&= a(M^2_{\pi p}) \sum_{m} \mu_m\ \ y^m_\ell(\xi,\omega)\,|JM_J\rangle,
\end{aligned}
$$

where the μ_m are Clebsch-Gordan coefficients, the $y^m_\ell(\xi,\omega)$ are spherical harmonics in the variables ξ and ω, $-\ell \leq m \leq \ell$, and $-J \leq M_J \leq J$. Expanding further, we get

$$
\begin{aligned}
|JM_J\rangle &= \sum_{M=M_J-M_S} \langle LM;\ \tfrac{1}{2}\ M_S|JM_J\rangle\,|LM\rangle\,|\tfrac{1}{2}\ M_S\rangle \\
&= \sum_{M} \nu_M\ Y^M_L(\theta,\phi)\ \chi^{M_S},
\end{aligned}
$$

where the ν_M are Clebsch-Gordan coefficients, the $Y^M_L(\theta,\phi)$ are spherical

harmonics in the variables θ and ϕ, $-L \leq M \leq L$, χ^{M_S} are the decay proton spin projectors, and $M_S = \pm 1/2$. Combining the two expansions, we have

$$(\ell\ L_J)_{\mathcal{J}} = a_{\alpha\beta}(M^2)_{\pi p} \sum_m \sum_M \mu_m \nu_M\ y_\ell^m(\xi, \omega) Y_L^M(\theta, \phi) \chi^{M_S},$$

where $\alpha = 0$ for $\ell = 0$ and $\alpha = 2\mathcal{J}$ for $\ell = 1$; $\beta = 0$ for $L = 0$ and $\beta = 2J$ for $L = 1$.

In terms of this expansion, the ten final state complex amplitudes are:

$$(sS_{1/2})_{1/2} = a_{00}\{\quad y_0^0 Y_0^0 \chi^{\pm 1/2}\},$$

$$(sP_{1/2})_{1/2} = a_{01}\{\mp(\tfrac{1}{3})^{1/2}\ y_0^0 Y_1^0 \chi^{\pm 1/2} \pm (\tfrac{2}{3})^{1/2}\ y_0^0 Y_1^{\pm 1} \chi^{\mp 1/2}\},$$

$$(sP_{3/2})_{3/2} = a_{03}\{\ (\tfrac{2}{3})^{1/2}\ y_0^0 Y_1^0 \chi^{\pm 1/2} + (\tfrac{1}{3})^{1/2}\ y_0^0 Y_1^{\pm 1} \chi^{\mp 1/2}\},$$

$$(pS_{1/2})_{1/2} = a_{10}\{\mp(\tfrac{1}{3})^{1/2}\ y_1^0 Y_0^0 \chi^{\pm 1/2} \pm (\tfrac{2}{3})^{1/2}\ y_1^{\pm 1} Y_0^0 \chi^{\mp 1/2}\},$$

$$(pS_{1/2})_{3/2} = a_{30}\{\ (\tfrac{2}{3})^{1/2}\ y_1^0 Y_0^0 \chi^{\pm 1/2} + (\tfrac{1}{3})^{1/2}\ y_1^{\pm 1} Y_0^0 \chi^{\mp 1/2}\},$$

$$(pP_{1/2})_{1/2} = a_{11}\{[-\tfrac{2}{3}\ y_1^{\pm 1} Y_1^{\mp 1} + \tfrac{1}{3}\ y_1^0 Y_1^0]\chi^{\pm 1/2} + [\tfrac{\sqrt{2}}{3}\ y_1^{\pm 1} Y_1^0 - \tfrac{\sqrt{2}}{3}\ y_1^0 Y_1^{\pm 1}]\chi^{\mp 1/2}\},$$

$$(pP_{1/2})_{3/2} = a_{31}\{[\mp\tfrac{\sqrt{2}}{3}\ y_1^{\pm 1} Y_1^{\mp 1} \mp \tfrac{\sqrt{2}}{3}\ y_1^0 Y_1^0]\chi^{\pm 1/2} + [\pm\tfrac{1}{3}\ y_1^{\pm 1} Y_1^0 \pm \tfrac{2}{3}\ y_1^0 Y_1^{\pm 1}]\chi^{\mp 1/2}\},$$

$$(pP_{3/2})_{1/2} = a_{13}\{[\ (\tfrac{1}{2})^{1/2}\ y_1^{\mp 1} Y_1^{\pm 1} - \tfrac{\sqrt{2}}{3}\ y_1^0 Y_1^0 - \tfrac{1}{3\sqrt{2}}\ y_1^{\pm 1} Y_1^{\mp 1}]\chi^{\pm 1/2} + [-\tfrac{1}{3}\ y_1^0 Y_1^{\pm 1} + \tfrac{1}{3}\ y_1^{\pm 1} Y_1^0]\chi^{\mp 1/2}\},$$

$$(pP_{3/2})_{3/2} = a_{33}\{[\pm(\tfrac{2}{5})^{1/2}\ y_1^{\mp 1} Y_1^{\pm 1} \pm \tfrac{1}{3}(\tfrac{2}{3})^{1/2}\ y_1^0 Y_1^0 \mp \tfrac{2}{3}(\tfrac{2}{5})^{1/2}\ y_1^{\pm 1} Y_1^{\mp 1}]\chi^{\pm 1/2} + [\pm\frac{1}{3(5)^{1/2}}\ y_1^0 Y_1^{\pm 1}$$

$$\mp \frac{4}{3(5)^{1/2}} \; y_1^{\pm 1} Y_1^0] \chi^{\mp 1/2} \},$$

$$(pP_{3/2})_{5/2} = a_{53} \{ [(\tfrac{1}{10})^{1/2} \; y_1^{\mp 1} Y_1^{\pm 1} + (\tfrac{2}{5})^{1/2} \; y_1^0 Y_1^0 + (\tfrac{1}{10})^{1/2} \; y_1^{\pm 1} Y_1^{\mp 1}] \chi^{\pm 1/2} + [\frac{1}{(5)^{1/2}} \; y_1^0 Y_1^{\pm 1} + \frac{1}{(5)^{1/2}} \; y_1^{\pm 1} Y_1^0] \chi^{\mp 1/2} \},$$

where the upper sign is used when the spin projection of the initial proton is +1/2, and the lower sign is used when the spin projection is -1/2. (All arguments have been suppressed.)

The matrix element is now the sum of these expanded complex amplitudes,

$$\mathcal{M}^{\pm} = \sum_{\substack{\ell = 0, 1 \\ L = 0, 1}} (\mathcal{J} + 1/2)^{1/2} \begin{pmatrix} -1 \\ +1 \end{pmatrix} \mathcal{J} + \mathcal{L} + 1/2 \times a_{\alpha\beta}(M_{\pi p}^2) \sum_m \sum_M \mu_m \nu_M \; y_\ell^m(\xi, \omega) Y_L^M(\theta, \phi) \chi^{\pm 1/2},$$

where $\mathcal{M}^+$ is that portion of the matrix element for $\mathcal{J}_z = +1/2$ and $\mathcal{M}^-$ is for $\mathcal{J}_z = -1/2$ and the factors dependent on $\mathcal{L}$ and $\mathcal{J}$ result from the expansion of an incoming plane wave into an outgoing spherical wave. The desired expression, Eq. (6), is $|\mathcal{M}|^2 = (\tfrac{1}{2})|\mathcal{M}^+|^2 + (\tfrac{1}{2})|\mathcal{M}^-|^2$.

We can now gather terms and write

$$\mathcal{M}^{\pm} = G^{\pm} \chi^{\pm 1/2} + H^{\pm} \chi^{\mp 1/2},$$

where

$$G^{\pm} = a_{00} \; y_0^0 Y_0^0 + (\tfrac{1}{3})^{1/2} (a_{10} + 2a_{30}) \; y_1^0 Y_0^0 + (\tfrac{1}{3})^{1/2} (a_{01} + 2a_{03}) \; y_0^0 Y_1^0 + \tfrac{1}{3}[(a_{11} + 2a_{31}) - \sqrt{2}(a_{13} + (\tfrac{2}{5})^{1/2} a_{33} - 3(\tfrac{3}{5})^{1/2} a_{53})] \; y_1^0 Y_1^0$$

$$- \frac{2}{3}\left[(a_{11} - a_{31}) - \frac{1}{2\sqrt{2}}(a_{13} + 4(\tfrac{2}{5})^{1/2} a_{33} + 3(\tfrac{3}{5})^{1/2} a_{53})\right] y_1^{\pm 1} Y_1^{\mp 1}$$
$$+ \frac{1}{\sqrt{2}}(a_{13} - 2(\tfrac{2}{5})^{1/2} a_{33} + (\tfrac{3}{5})^{1/2} a_{53})\, y_1^{\mp 1} Y_1^{\pm 1},$$

$$H^{\pm} = -(\tfrac{2}{3})^{1/2}(a_{10} - a_{30})\, y_1^{\pm 1} Y_0^0$$
$$- (\tfrac{2}{3})^{1/2}(a_{01} - a_{03})\, y_0^0 Y_1^{\pm 1}$$
$$- \frac{\sqrt{2}}{3}\left[(a_{11} + 2a_{31}) + \frac{1}{\sqrt{2}}(a_{13} + (\tfrac{2}{5})^{1/2} a_{33} - 3(\tfrac{3}{5})^{1/2} a_{53})\right] y_1^0 Y_1^{\pm 1}$$
$$+ \frac{\sqrt{2}}{3}\left[(a_{11} - a_{31}) + \frac{1}{\sqrt{2}}(a_{13} + 4(\tfrac{2}{5})^{1/2} a_{33} + 3(\tfrac{3}{5})^{1/2} a_{53})\right] y_1^{\pm 1} Y_1^0.$$

We note that upon taking the absolute square of the amplitudes $G^{\pm}$ and $H^{\pm}$, the variables ϕ and ω always appear in the combination $(\phi - \omega)$. As defined by the spherical harmonics, ϕ and ω are measured with respect to some coordinate system fixed in space. The angle ω is the azimuthal angle of the production plane in space; it is of no interest in this experiment. What is of interest is the angle $(\phi - \omega)$, the azimuthal angle of the decay proton with respect to the production plane. We therefore redefine the angle $(\phi - \omega)$ as ϕ.

The absolute square of the matrix element, $|\mathcal{M}|^2$, is now obtained by taking the absolute square of $G^{\pm}$ and $H^{\pm}$. That is,

$$|\mathcal{M}|^2 = \frac{1}{2}|\mathcal{M}^+|^2 + \frac{1}{2}|\mathcal{M}^-|^2$$
$$= \frac{1}{2}\{|G^+|^2 + |H^+|^2 + |G^-|^2 + |H^-|^2\}. \qquad \text{(A1)}$$

Gathering terms that have the same angular dependence, we have

$$|\mathcal{M}|^2 = \sum_{i=1}^{14} C_i(M_{\pi p}^2)\, \tfrac{1}{2}\left[y_\ell^m(\xi, 0) Y_L^{-M}(\theta, \phi) + y_\ell^{-m}(\xi, 0) Y_L^M(\theta, \phi)\right]_i$$
$$= C_i\, y_0^0 Y_0^0 + C_2\, y_1^0 Y_0^0 + C_3\, y_0^0 Y_1^0$$

$$
\begin{aligned}
&+ C_4\ y_1^0 Y_1^0 + C_5 \tfrac{1}{2}(\ y_1^1 Y_1^{-1} + y_1^{-1} Y_1^1) \\
&+ C_6\ y_2^0 Y_0^0 + C_7\ y_0^0 Y_2^0 \\
&+ C_8\ y_2^1 Y_1^0 + C_9 \tfrac{1}{2}(\ y_2^1 Y_1^{-1} + \ y_2^{-1} Y_1^1) \\
&+ C_{10}\ y_1^0 Y_2^0 + C_{11} \tfrac{1}{2}(\ y_1^1 Y_2^{-1} + \ y_1^{-1} Y_2^1) \\
&+ C_{12}\ y_2^0 Y_2^0 + C_{13} \tfrac{1}{2}(\ y_2^1 Y_2^{-1} + \ y_2^{-1} Y_2^1) \\
&+ C_{14} \tfrac{1}{2}(\ y_2^2 Y_2^{-2} + \ y_2^{-2} Y_2^2), \qquad (6)
\end{aligned}
$$

where the fourteen C's are real functions of $M_{\pi p}^2$ resulting from combinations of the various complex $a_{\alpha\beta}$'s. The dependence of each $C_i(M_{\pi p}^2)$ on the $a_{\alpha\beta}(M_{\pi p}^2)$'s is given in Table AII. If we are not interested specifically in the values of $\mathcal{J}$ (the total angular momentum of the state) and J (the total angular momentum of the final π-p state), we can look at the <u>type</u> of terms, $\langle \ell L | \ell' L' \rangle$, which comprise each $C_i(M_{\pi p}^2)$. These terms are listed in Table IV for each $C_i(M_{\pi p}^2)$. For example, from Table AII we see that $C_4 = (2/3)\langle (a_{10} + 2a_{30}) | (a_{01} + 2a_{03}) \rangle + (2/3)\langle a_{00} | (a_{11} + 2a_{31}) - \sqrt{2}\,(a_{13} + (2/5)^{1/2} a_{33} - 3(3/5)^{1/2} a_{53} \rangle$. If we are not interested in the values of $\mathcal{J}$ and J, we see that C_4 consists of terms of the type $\langle pS | sP \rangle$ and $\langle sS | pP \rangle$.

In Section V we show that the only complex amplitudes which need to be considered are $(sS_{1/2})_{1/2}$, $(sP_{3/2})_{3/2}$, and $(pS_{1/2})_{1/2}, 3/2$. Thus $G^{\pm}$ and $H^{\pm}$ simplify to

$$
\begin{aligned}
G^{\pm} &= a_{00} + (a_{10} + 2a_{30}) \cos\xi + 2a_{03} \cos\theta, \\
H^{\pm} &= (a_{10} - a_{30}) \sin\xi\ e^{\pm i\omega} - a_{03} \sin\theta\ e^{\pm i\phi}, \qquad (A2)
\end{aligned}
$$

and each $C_i(M^2_{\pi p})$ simplifies considerably; all terms in Table AII and Table IV which are shaded become zero. We therefore have:

$$C_1 = |a_{00}|^2 + 2|a_{03}|^2 + |a_{10}|^2 + 2|a_{30}|^2,$$

$$C_2 = \frac{2}{\sqrt{3}} \text{Re}\,(a^*_{00} a_{10} + 2a^*_{00} a_{30}),$$

$$C_3 = \frac{4}{\sqrt{3}} \text{Re}\,(a^*_{00} a_{03}),$$

$$C_4 = \frac{4}{3} \text{Re}\,(a^*_{10} a_{03} + 2a^*_{30} a_{03}),$$

$$C_5 = \frac{4}{3} \text{Re}\,(a^*_{10} a_{03} - a^*_{30} a_{03}),$$

$$C_6 = \frac{2}{5^{1/2}} |a_{30}|^2 + \frac{4}{5^{1/2}} \text{Re}\,(a^*_{10} a_{30}),$$

$$C_7 = \frac{2}{5^{1/2}} |a_{03}|^2 .$$

Expressing each complex $a_{\alpha\beta}(M^2_{\pi p})$ in terms of $[A_{\alpha\beta}]$ [kinematical factor] $[e^{i\lambda_{\alpha\beta}}]$, as prescribed in Section V, we obtain Eq. (9).

B. Inclusion of $N^*(1550) \to \eta p$ Resonance Amplitudes in the Matrix Element

In Appendix A we show that

$$G^{\pm} = a_{00} + (a_{10} + 2a_{30}) \cos\xi + 2a_{03} \cos\theta ,$$
$$H^{\pm} = (a_{10} - a_{30}) \sin\xi\, e^{\pm i\omega} - a_{03} \sin\theta\, e^{\pm i\phi} , \qquad \text{(A2)}$$

if we consider only the complex amplitudes $(sS_{1/2})_{1/2}$, $(sP_{3/2})_{3/2}$, and $(pS_{1/2})_{1/2,\,3/2}$. All quantities are referred to the $(\pi\text{-}p)$ rest frame and are defined in Appendix A.

In addition to the above amplitudes we also want to consider s'- and p'-wave production of the S'-wave resonance, the $N^*(1550) \to \eta p$. (We will use primes to indicate quantities referred to the η-p rest frame in the same way that the unprimed quantities are referred to the π-p rest frame.) Production via d'-wave and higher need not be considered since these waves produce terms in $\cos^3\xi$ and higher, $\cos^3\theta$ and higher, and $\cos^2\phi$ and higher; these higher order terms are not required by the data. Adding amplitudes $(s'S'_{1/2})_{1/2}$ and $(p'S'_{1/2})_{1/2,\,3/2}$ to Eq. (A2), we have

$$G^{\pm} = (a_{00} + a'_{00}) + (a_{10} + 2a_{30})\cos\xi + (a'_{10} + 2a'_{30})\cos\xi' + 2a_{03}\cos\theta,$$

$$H^{\pm} = (a_{10} - a_{30})\sin\xi\, e^{\pm i\omega} + (a'_{10} - a'_{30})\sin\xi'\, e^{\pm i\omega'} - a_{03}\sin\theta\, e^{\pm i\phi}.$$

By Eq. (A1),

$$\begin{aligned}
|\mathcal{M}|^2 = {} & (a_{00}^2 + 2a_{00}a'_{00} + a'^2_{00}) \\
& + (a_{10}^2 - 2a_{10}a_{30} + a_{30}^2) \\
& + (a'^2_{10} - 2a'_{10}a'_{30} + a'^2_{30}) \\
& + a_{03}^2(1 + 3\cos^2\theta) \\
& + (6a_{10}a_{30} + 3a_{30}^2)\cos^2\xi \\
& + (6a'_{10}a'_{30} + 3a'^2_{30})\cos^2\xi' \\
& + (2a_{10}a'_{10} + 4a_{10}a'_{30} + 4a_{30}a'_{10} + 8a_{30}a'_{30})\cos\xi\cos\xi' \\
& + (2a_{10}a'_{10} - 2a_{10}a'_{30} - 2a_{30}a'_{10} + 2a_{30}a'_{30})\sin\xi\sin\xi'\cos(\omega-\omega') \\
& + (2a_{00}a_{10} + 4a_{00}a_{30} + 2a'_{00}a_{10} + 4a'_{00}a_{30})\cos\xi \\
& + (2a_{00}a'_{10} + 4a_{00}a'_{30} + 2a'_{00}a'_{10} + 4a'_{00}a'_{30})\cos\xi'
\end{aligned}$$

$$+ (4a_{00}a_{03} + 4a'_{00}a_{03}) \cos\theta$$

$$+ (4a_{10}a_{03} + 8a_{30}a_{03}) \cos\xi \cos\theta$$

$$+ (4a'_{10}a_{03} + 8a'_{30}a_{03}) \cos\xi' \cos\theta$$

$$+ (-2a_{10}a_{03} + 2a_{30}a_{03}) \sin\xi \sin\theta \cos(\omega-\phi)$$

$$+ (-2a'_{10}a_{03} + 2a'_{30}a_{03}) \sin\xi' \sin\theta \cos(\omega'-\phi), \qquad \text{(B1)}$$

where we use the shorthand notation $a^2_{\alpha\beta} = |a_{\alpha\beta}|^2$ and $a_{\alpha\beta} a_{\alpha'\beta'} = \mathrm{Re}\{a^*_{\alpha\beta} a_{\alpha'\beta'}\}$.

In Eq. (B1) we have a mixed set of variables. So that we may know which quantities belong in which C_i, the variables $\cos\xi'$, $\sin\xi'\cos\omega'$, and $\sin\xi'\sin\omega'$ must be expressed in terms of the independent variables $\cos\xi$, $\cos\theta$, and ϕ. As in Appendix A, we define the azimuthal angle ω to be zero, thereby defining the plane of reference.

In order to express $\cos\xi'$ in terms of the independent angles, we note that by Lorentz transformation

$$\underset{\sim}{q} = \underset{\sim}{p}' + \underset{\sim}{\beta}\left[\frac{(\underset{\sim}{p}' \cdot \underset{\sim}{\beta})(\gamma-1)}{\beta^2} - \gamma\epsilon_\pi\right], \qquad \text{(B2)}$$

where $\underset{\sim}{p}$ and ϵ_π are the momentum and energy, respectively, of the pion in the center of mass, and

$$\beta = -\frac{\underset{\sim}{p}}{E-\epsilon_\eta},$$

$$\gamma = \frac{E-\epsilon_\eta}{M}, \qquad \text{(B3)}$$

$$\epsilon_\eta = (p^2 + m_\eta^2)^{1/2}.$$

Using Eq. (B3) and the fact that $p^2 = (E-\epsilon_\eta)^2 - M^2 = (E-\epsilon_\eta+M)(E-\epsilon_\eta-M)$, $E_\pi = \gamma(\epsilon_\pi - \underset{\sim}{\beta}\cdot\underset{\sim}{p}')$, we get $\underset{\sim}{q} = \underset{\sim}{p}' + \tau\underset{\sim}{p}$, where $\tau = (\epsilon_\pi + E_\pi)/(E-\epsilon_\eta+M)$. Therefore

$$\hat{p}' = \frac{q}{p'}\,\hat{q} - (\tau\frac{p}{p'})\,\hat{p}\,. \tag{B4}$$

The z axis, the direction of the beam in the center of mass, is common to both the primed and unprimed coordinate systems. Therefore taking the z component of Eq. (B4), we get

$$\cos\xi' = (\frac{q}{p'})\cos\theta - (\frac{p\tau}{p'})\cos\xi\,. \tag{B5}$$

To obtain the other two angular quantities we need the following space angle relationships,

$$\hat{p}\cdot\hat{q} = \cos\xi\cos\theta + \sin\xi\sin\theta\cos\phi, \tag{B6}$$

$$\hat{p}'\cdot\hat{q} = \cos\xi'\cos\theta + \sin\xi'\sin\theta\cos(\phi-\omega'), \tag{B7}$$

$$\hat{p}\cdot\hat{p}' = \cos\xi\cos\xi' + \sin\xi\sin\xi'\cos\omega'. \tag{B8}$$

Now equate Eq. (B8) with p dotted with Eq. (B4) and use Eqs. (B6) and (B5) to get

$$\sin\xi'\cos\omega' = (\frac{q}{p'})\sin\theta\cos\phi - (\tau\frac{p}{p'})\sin\xi. \tag{B9}$$

To obtain the other angular quantity equate Eq. (B7) with q dotted with Eq. (B4) and use Eqs. (B5), (B7), and (B9) to get

$$\sin\xi\sin\omega' = (\frac{q}{p'})\sin\theta\sin\phi. \tag{B10}$$

We now put Eqs. (B5), (B9), and (B10) into Eq. (B1) and—converting to spherical harmonics—we obtain the quantities $C_i(M^2, M'^2)$:

$$C_1(M^2, M'^2) = \{(a_{00}^2 + 2a_{03}^2 + a_{10}^2 + 2a_{30}^2)$$
$$+ (a_{00}'^2 + 2a_{00}a_{00}')$$
$$+ (4a_{03}a_{30}') \frac{q}{p'}$$
$$- (2a_{10}a_{10}' + 4a_{30}a_{30}') \frac{\tau p}{p'}$$
$$+ (a_{10}'^2 + 2a_{30}'^2)[(\frac{q}{p'})^2 + (\frac{\tau p}{p'})^2]\} ,$$

$$C_2(M^2, M'^2) = \{(2a_{00}a_{10} + 4a_{00}a_{30}) + (2a_{00}'a_{10} + 4a_{00}'a_{30})$$
$$- (2a_{00}a_{10}' + 4a_{00}a_{30}' + 2a_{00}'a_{10}' + 4a_{00}'a_{30}') \frac{\tau p}{p'}\} \frac{1}{\sqrt{3}} ,$$

$$C_3(M^2, M'^2) = \{(4a_{00}a_{03}) + (4a_{00}'a_{03})$$
$$+ (2a_{00}a_{10}' + 4a_{00}a_{30}' + 2a_{00}'a_{10}' + 4a_{00}'a_{30}') \frac{q}{p'}\} \frac{1}{\sqrt{3}} ,$$

$$C_4(M^2, M'^2) = \{(4a_{03}a_{10} + 8a_{03}a_{30})$$
$$- (4a_{03}a_{10}' + 8a_{03}a_{30}') \frac{\tau p}{p'}$$
$$+ (2a_{10}a_{10}' + 4a_{10}a_{30}' + 4a_{10}'a_{30} + 8a_{30}a_{30}') \frac{q}{p'}$$
$$- (2a_{10}'^2 + 8a_{10}'a_{30}' + 8a_{30}'^2) \frac{\tau pq}{p'^2}\} \frac{1}{3} ,$$

$$C_5(M^2, M'^2) = \{(4a_{03}a_{10} - 4a_{03}a_{30})$$
$$- (4a_{03}a_{10}' - 4a_{03}a_{30}') \frac{\tau p}{p'}$$
$$+ (-4a_{10}a_{10}' + 4a_{10}a_{30}' + 4a_{10}'a_{30} - 4a_{30}a_{30}') \frac{q}{p'}$$
$$- (-4a_{10}'^2 + 8a_{10}'a_{30}' - 4a_{30}'^2) \frac{\tau pq}{p'^2}\} \frac{1}{3} ,$$

$$C_6(M^2, M'^2) = \{(2a_{10}a_{30} + a_{30}^2)$$
$$+ (2a_{10}'a_{30}' + a_{30}'^2) \frac{\tau^2 p^2}{p'^2}$$
$$- (2a_{10}a_{30}' + 2a_{10}'a_{30} + 2a_{30}a_{30}') \frac{\tau p}{p'}\} \frac{2}{5^{1/2}} ,$$

$$C_7(M^2, M'^2) = \{(a_{03}^2) + (2a_{03}a'_{10} + 2a_{03}a'_{30})\frac{q}{p'} + (2a'_{10}a'_{30} + a'^2_{30})\frac{q^2}{p'^2}\}\frac{2}{5^{1/2}} .$$

We now need the M^2 dependence of the a factors, and the M'^2 dependence of the a' factors. For the π^+p data the M^2 dependence is given in Section V and the M'^2 dependence is as follows:

$$\begin{aligned} a'_{00}(M'^2) &= A'_{00}\, e^{i\lambda'_{00}}\, k\,(M'/q'\Gamma')^{1/2}\left[\frac{(1-x)^{1/2}}{\epsilon' - i}\right], \\ a'_{10}(M'^2) &= A'_{10}\, e^{i\lambda'_{10}}\, p'\,(M'/q'\Gamma')^{1/2}\left[\frac{(1-x)^{1/2}}{\epsilon' - i}\right], \\ a'_{30}(M'^2) &= A'_{30}\, e^{i\lambda'_{30}}\, p'\, k^2\,(M'/q'\Gamma')^{1/2}\left[\frac{(1-x)^{1/2}}{\epsilon' - i}\right], \end{aligned} \qquad \text{(B12)}$$

where[23] $\epsilon' = (M_0^2 - M'^2)^2/\Gamma' M_0$, $\Gamma' = \Gamma_0(q'/q_0)(M'/M_0)^{-1}$, with (Ref. 13) $M_0 = 1550$ MeV, $\Gamma_0 = 130$ MeV, $x = 0.30$, and q_0 the value of q' at resonance.

Substituting Eqs. (11) and (B12) into Eq. (B11) gives $C_i(M^2, M'^2)$ explicitly in terms of the $A_{\alpha\beta}$, $A'_{\alpha\beta}$, $\lambda_{\alpha\beta}$, $\lambda'_{\alpha\beta}$, and various momentum dependences. Now, integration over M'^2, one variable of the production Dalitz plot, gives the C_i's in terms of the other variable, M^2. Treating these new expressions as described in Section V, we can fit the π^+p data and determine the quantities, A'_{00}, A'_{10}, A'_{30}, λ'_{00}, λ'_{10}, λ'_{30}.

For the π^-p data we make the substitution $A'_{\alpha\beta}\, e^{i\lambda'_{\alpha\beta}} \rightarrow (1/3)A'_{\alpha\beta}\, e^{i\lambda'_{\alpha\beta}} + (2/3)B'_{\alpha\beta}\, e^{i\nu'_{\alpha\beta}}$ and $A_{\alpha\beta}\, e^{i\lambda_{\alpha\beta}} \rightarrow (1/3)A_{\alpha\beta}\, e^{i\lambda_{\alpha\beta}}$ except that $A_{00}\, e^{i\lambda_{00}} \rightarrow (1/3)A_{00}\, e^{i\lambda_{00}} + (2/3)B_{00}\, e^{i\nu_{00}}$. Now fitting the π^-p data, we obtain the quantities, $B'_{\alpha\beta}$ and $\nu'_{\alpha\beta}$.

FOOTNOTES AND REFERENCES

*Work done under the auspices of the U. S. Atomic Energy Commission.

1. A. Pevsner, R. Kraemer, M. Nussbaum, C. Richardson, P. Schlein, R. Strand, T. Toohig, M. Block, A. Engler, R. Gessaroli, and C. Meltzer, Phys. Rev. Letters 7, 421 (1961). See also Pierre L. Bastien, J. Peter Berge, Orin I. Dahl, Massimiliano Ferro-Luzzi, Donald H. Miller, Joseph J. Murray, Arthur H. Rosenfeld, and Mason B. Watson, Phys. Rev. Letters 8, 114 (1962); D. Duane Carmony, Arthur H. Rosenfeld, and Remy T. Van de Walle, Phys. Rev. Letters 8, 117 (1962); Arthur H. Rosenfeld, D. Duane Carmony, and Remy T. Van de Walle, Phys. Rev. Letters 8, 293 (1962); M. Chrétien, F. Bulos, H. R. Crouch, Jr., R. E. Lanou, Jr., J. T. Massimo, A. M. Shapiro, J. A. Averell, C. A. Bordner, Jr., A. E. Branner, D. R. Firth, M. E. Law, E. E. Ronat, K. Strauch, J. C. Street, J. J. Szymanski, A. Weinberg, B. Nelson, I. A. Pless, L. Rosenson, G. A. Salandin, R. K. Yamamoto, L. Guerriero, and F. Waldner, Phys. Rev. Letters 9, 127 (1962).

2. Horst W. J. Foelsche and Henry L. Kraybill, Phys. Rev. 134, B1138 (1964).

3. P. Daronian, A. Daudin, M. A. Jabiol, C. Lewin, C. Kochowski, B. Ghidini, S. Mongelli, and V. Picciarelli, Nuovo Cimento 41, 502 (1966).

4. Frederick E. James and Henry L. Kraybill, Phys. Rev. 142, 896 (1966).

5. C. Alff, D. Berley, D. Colley, N. Gelfand, U. Nauenberg, D. Miller, J. Schultz, J. Steinberger, T. H. Tan, H. Brugger,

P. Kramer, and R. Plano, Phys. Rev. Letters 9, 322, 325 (1962); C. Alff-Steinberger, D. Berley, D. Colley, N. Gelfand, D. Miller, U. Nauenberg, J. Schultz, T. H. Tan, H. Brugger, P. Kramer, and R. Plano, Phys. Rev. 145, 1072 (1966).

6. Maris Abolins, Richard L. Lander, Werner A. W. Melhop, Nguyen-huu Xuong, and Philip M. Yager, Phys. Rev. Letters 11, 381 (1963).

7. Benjamin Ching-Chun Shen, Lawrence Radiation Laboratory Report UCRL-16170, September 1965 (unpublished).

8. D. D. Carmony, F. Grard, R. T. Van de Walle, and Nguyen-huu Xuong, Proceedings of CERN International Conference on High-Energy Physics, p. 44 (1962).

9. P. H. Satterbloom, W. D. Walker, and A. R. Irwin, Phys. Rev. 134, B207 (1964).

10. Suh Urk Chung, Orin I. Dahl, Janos Kirz, and Donald H. Miller, Phys. Rev. 165, 1491 (1968).

10a. G. Ascoli, H. B. Crawley, D. W. Mortara, A. Shapiro, C. A. Bridges, B. I. Eisenstein, U. E. Kruse, E. D. Schafer, and B. Terreault, Phys. Rev. Letters 20, 1321 (1968).

11. Leo Stodolsky and J. J. Sakurai, Phys. Rev. Letters 11, 90 (1963); Leo Stodolsky, Phys. Rev. 134, B1099 (1964).

12. R. Levrat, C. A. Tolstrup, P. Schübelin, C. Nef, M. Martin, B. C. Maglić, W. Kienzle, M. N. Focacci, L. Dubal, and G. Chikovani, Phys. Letters 22, 714 (1966); G. Ch kovani, M. N. Focacci, W. Kienzle, C. Lechanoine, B. Levrat, B. Maglić, M. Martin, P. Schüberlin, L. Dubal, M. Fisher, P. Grieder, H. A. Neal, and C. Nef, Phys. Letters 25, B44 (1967); D. R. O. Morrison, Phys. Letters 25, B238 (1967).

13. Arthur H. Rosenfeld, Naomi Barash-Schmidt, Angela Barbaro-Galtieri, LeRoy R. Price, Paul Söding, Charles G. Wohl, Matts Roos, and William J. Willis, Rev. Mod. Phys. 40, 77 (1968).

14. J. Alitti, J. P. Baton, B. Deler, M. Neveu-Rene, J. Crussard, J. Ginestet, A. H. Tran, R. Gessaroli, A. Romano, Phys. Letters 15, 69 (1965); see also A. Astier, J. Cohen-Ganouna, M. Della Negra, B. Maréchal, L. Montanet, M. Tomas, M. Baubillier, J. Duboc, Phys. Letters 25, B294 (1967).

15. Sanford E. Wolf, Norbert Schmitz, Lester J. Lloyd, William Laskar, Frank S. Crawford, Jr., Janice Button, Jared A. Anderson, and Gideon Alexander, Rev. Mod. Phys. 33, 439 (1961).

16. The beam contaminations have been determined by: Fernand Grard and Gerald A. Smith, Phys. Rev. 127, 607 (1962) for the 1050-MeV/c π^+ data; Frank S. Crawford, Jr., Fernand Grard, and Gerald A. Smith, Phys. Rev. 128, 368 (1962) for the 1170-MeV/c π^+ data; Jared A. Anderson, Lawrence Radiation Laboratory Report UCRL-10838, May 1963, for the 1170-MeV/c π^- data.

17. Most of these events have been analyzed previously in regard to eta decay. See: Earle C. Fowler, Frank S. Crawford, Jr., L. J. Lloyd, Ronald A. Grossman, and LeRoy R. Price, Phys. Rev. Letters 10, 110 (1963); Frank S. Crawford, Jr., L. J. Lloyd, and Earle C. Fowler, Phys. Rev. Letters 10, 546 (1963); Frank S. Crawford, Jr., Ronald A. Grossman, L. J. Lloyd, and LeRoy R. Price, Phys. Rev. Letters 11, 564 (1963); Columbia-Berkeley-Purdue-Wisconsin-Yale Collaboration, Phys. Rev. 149, 1044 (1966).

18. G. R. Lynch, Program FAKE: Monte Carlo Simulation of Bubble Chamber Events, Lawrence Radiation Laboratory Report UCRL-10335, July 1962. This program generates "bubble chamber events" by a Monte Carlo method. These events are then sent through the

same programs used for the real events. In this manner one can easily calculate the effects of any set of correlated or uncorrelated cutoffs.

19. The attenuation due to strong interactions is based on $\pi^+ p$ total cross sections of 27.04 ± 0.80 mb and 29.69 ± 0.44 mb at 1050 and 1170 MeV/c, respectively, determined by Thomas J. Devlin, Burton J. Moyer, and Victor Perez-Mendez, Phys. Rev. 125, 690 (1962), and a $\pi^- p$ total cross section of 37.30 ± 0.55 mb at 1170 MeV/c determined by B. Amblard, P. Borgeaud, Y. Ducros, P. Falk-Vairiant, O. Guisan, W. Laskar, P. Sonderugger, A. Stirling, M. Yvert, A. Tran Ha, and S. D. Warshaw, Phys. Letters 10, 138 (1964).

20. The lab quantities were first transformed to the center of mass and then to the $\tilde{N}$ rest frame. Because of the nonlinearity of velocity addition in the Lorentz transformation, the z axis obtained by this procedure differs by a small rotation from that obtained by transforming from the laboratory to the $\tilde{N}$ rest frame directly.

21. Since parity is conserved in strong interactions, the ϕ distributions have been folded about 180 deg.

22. The factor $(M/q)^{1/2}$ arises from dividing out the two-body phase space factor; the factor $1/(\Gamma)^{1/2}$ appears because we choose the model in which the Δ is made "directly" in the same strong reaction in which the eta is made. If we choose the model in which the three final state particles are made directly and then the Δ is formed by "rescattering," the $(\Gamma)^{1/2}$ factor would not appear.

23. J. D. Jackson, Nuovo Cimento 34, 1644 (1964).

24. In order to convert from $\eta \to \pi^+\pi^-\pi^0$ decay to $\eta \to$ all decays, multiply the magnitudes by $1/(R)^{1/2}$, where $R = \Gamma(\eta \to \pi^+\pi^-\pi^0)/\Gamma(\eta \to \text{all})$. In order to convert the magnitude values to fermis, divide out the radius of interaction.

25. It is interesting to note that the fact that there are no interference terms between one partial wave and another in the cross-section expression, D_1, is a general result and not a consequence of the particular partial waves chosen. (For example, see Table AII.) In order for D_1, and hence the mass distributions $d\sigma/dM^2_{\pi p}$ and $d\sigma/dM^2_{\eta p}$, to exhibit interference terms, one of two conditions must exist. The first is the presence of two or more amplitudes which belong to the same partial wave, such as resonant and non-resonant amplitudes or two or more amplitudes of different I-spin. There will then be interference terms arising from these amplitudes of the same partial wave. The second condition which gives rise to interference terms is that the matrix element consists of both an amplitude which is a function of M^2 (one projection of the production Dalitz plot) and M'^2 (another projection of the Dalitz plot). (See Appendix B.) There will then be interference terms between amplitudes of M^2 and amplitudes of M'^2 which come from the same initial state $\mathcal{L}_J$.

26. P. Auvil, C. Lovelace, A. Donnachie, and A. T. Lea, Phys. Letters 12, 76 (1964); 19, 148 (1965); P. Bareyre, C. Brickman, A. V. Sterling, and G. Villet, Phys. Letters 18, 342 (1965); R. J. Cence, Phys. Letters 20, 306 (1966); L. D. Roper, R. M. Wright, and B. T. Feld, Phys. Rev. 138, B190 (1965); B. H. Bransden,

P. J. O'Donnell, and R. G. Moorhouse, Phys. Rev. 139, B1566 (1965); Proc. Roy. Soc. (London) A289, 538 (1966); Phys. Letters 19, 420 (1965).

27. F. Bulos, R. E. Lanou, A. E. Pifer, A. M. Shapiro, M. Widgoff, R. Panvini, A. E. Brenner, C. A. Bordner, M. E. Law, E. E. Ronat, K. Strauch, J. J. Szymanski, P. Bastien, B. B. Brabson, Y. Eisenberg, B. T. Feld, V. K. Fisher, I. A. Pless, L. Rosenson, R. K. Yamamoto, G. Calvelli, L. Guerriero, G. A. Salandin, A. Tomasin, L. Ventura, C. Voci, and F. Waldner, Phys. Rev. Letters 13, 486 (1964); W. Bruce Richards, Charles B. Chiu, Richard D. Eandi, A. Carl Helmholz, Robert W. Kenny, Burton J. Moyer, John A. Poirier, Robert J. Cence, Vincent Z. Peterson, Narender K. Sehgal, and Victor J. Stenger, Phys. Rev. Letters 16, 1221 (1966); F. Uchiyama-Campbell and R. K. Logan, Phys. Rev. 149, 1220 (1966); C. Bacci, G. Penso, G. Salvini, C. Mencuccini, and V. Silvestrini, Nuovo Cimento 45, 983 (1966); W. G. Jones, D. M. Binnie, A. Duane, J. P. Horsey, D. C. Mason, J. A. Newth, I. U. Rahman, J. Walters, N. Horwitz, and P. Palit, Phys. Letters 23, 597 (1966); R. Prepost, D. Lundquist, and D. Quinn, Phys. Rev. Letters 18, 82 (1967).

28. G. Bassompierre, Y. Goldschmidt-Clermont, A. Grant, V. P. Henri, B. Jongejans, R. L. Lander, D. Linglin, F. Muller, J. M. Perreau, R. Sekulin, W. De Baere, J. Debaisieux, P. DuFour, F. Grard, J. Heughebaert, L. Pape, P. Peeters, F. Verbeure, and R. Windmolders, Phys. Letters 25B, 440 (1967).

Table I. Scanning information and partial cross sections for $\pi p \to \pi p \eta$, $\eta \to \pi^+\pi^-\pi^0$.

	$\pi^+ p \to \pi^+ p \eta$ $\eta \to \pi^+\pi^-\pi^0$ 1170 MeV/c	$\pi^- p \to \pi^- p \eta$ $\eta \to \pi^+\pi^-\pi^0$ 1170 MeV/c		$\pi^+ p \to \pi^+ p \eta$ $\eta \to \pi^+\pi^-\pi^0$ 1050 MeV/c
		Part I	Part II	
Total number of pictures scanned	34 928	18 309	81 858	98 291
Beam tracks per frame	17.22 ± 0.39	17.4 ± 0.5	14.90 ± 0.21	13.76 ± 0.90
Length of beam track in fiducial volume	(157.3 ± 0.1) cm	145 cm	147.8 cm	(157.3 ± 0.1) cm
Total track length scanned (uncorrected)	$(94.61 \pm 2.14) \times 10^6$ cm	$(46.19 \pm 1.32) \times 10^6$ cm	$(180.27 \pm 2.51) \times 10^6$ cm	$(212.75 \pm 13.92) \times 10^6$ cm
Beam contamination[a]	$(5.1 \pm 2.0)\%$	$(3.0 \pm 1.6)\%$	$(3.0 \pm 1.6)\%$	$(6.7 \pm 2.1)\%$
Attenuation due to strong interactions[b]	7.6%	8.6%	8.6%	6.8%
Total corrected track length	$(82.96 \pm 2.56) \times 10^6$ cm	$(40.95 \pm 1.35) \times 10^6$ cm	$(159.82 \pm 3.45) \times 10^6$ cm	$(185.00 \pm 12.82) \times 10^6$ cm
Number of observed events	135	87		51
Scanning efficiency	$(95.0 \pm 1.9)\%$	$(85.1 \pm 3.8)\%$		$(90.4 \pm 4.3)\%$
Selection criteria efficiency	91.5%	91.5%		91.5%
Number of corrected events	155.0 ± 13.7	111.4 ± 12.9		61.4 ± 9.1
Partial cross section	$(53.3 \pm 5.0)\mu b$	$(15.9 \pm 1.9)\mu b$		$(9.5 \pm 1.5)\mu b$

[a] Ref. 16.

[b] Ref. 19.

Table II. Partial cross sections for $\pi p \to \pi p \eta$, $\eta \to \pi^+\pi^-\pi^0$ in mb.

Incident beam momentum (BeV/c)	$\pi^+ p \to \pi^+ p \eta$, $\eta \to \pi^+\pi^-\pi^0$	$\pi^- p \to \pi^- p \eta$, $\eta \to \pi^+\pi^-\pi^0$
1.05[a]	0.0095 ± 0.0015	
1.17[a]	0.0533 ± 0.0050	0.0159 ± 0.0019
1.22[b]	0.069 ± 0.010	
1.39[b]	0.130 ± 0.045	
1.59[c]	0.12 ± 0.02	
2.03[h]		0.031 ± 0.010
2.08[d]	0.15 ± 0.03	
2.08[i]		0.037 ± 0.015
2.34[e]	0.23 ± 0.05	
2.62[e]	0.18 ± 0.09	
2.9[e]	0.15 ± 0.05	
3.2[j]		0.030 ± 0.010
3.43[f]	0.09 ± 0.04	
3.54[f]	0.07 ± 0.02	
3.65[g]	0.06 ± 0.02	
4.2[j]		0.021 ± 0.007

[a] This experiment.
[b] See Ref. 2.
[c] See Ref. 3.
[d] See Ref. 4.
[e] See Ref. 5.
[f] See Ref. 6.
[g] See Ref. 7.
[h] See Ref. 8.
[i] See Ref. 9.
[j] See Ref. 10.

Table III. Values of the D_i's in μb. The values D_8 through D_{14} (the shaded region) would be zero if our final choice of amplitudes were correct.

	1050-MeV/c π^+		1170-MeV/c π^+		1170-MeV/c π^-	
	1a	1b	2a	2b	3a	3b
	Experimental values	Fitted values	Experimental values	Fitted values	Experimental values	Fitted values
D_1	9.50 ± 1.51	7.55	53.30 ± 5.02	54.92	15.85 ± 1.91	16.13
D_2	-1.14 ± 1.12	0.50	5.71 ± 4.49	1.12	2.90 ± 1.63	0.73
D_3	-3.31 ± 1.49	-1.23	-12.47 ± 4.89	-15.38	-0.79 ± 1.71	-1.03
D_4	-0.35 ± 1.27	0.20	5.16 ± 4.95	1.01	0.08 ± 1.70	0.11
D_5	-0.46 ± 1.46	-1.63	-22.01 ± 4.63	-20.44	-3.03 ± 1.85	-2.27
D_6	-3.05 ± 1.25	-0.46	-2.51 ± 4.11	-2.78	-1.34 ± 1.65	-0.31
D_7	2.76 ± 1.47	1.98	8.26 ± 4.75	17.99	0.25 ± 1.63	2.00
D_8	3.46 ± 1.39		3.33 ± 4.36		-1.66 ± 1.71	
D_9	0.25 ± 1.25		3.84 ± 4.90		-0.68 ± 1.86	
D_{10}	0.63 ± 1.26		-2.88 ± 4.78		-0.57 ± 1.59	
D_{11}	-1.31 ± 1.45		4.02 ± 4.90		1.47 ± 1.98	
D_{12}	-0.68 ± 1.42		3.47 ± 4.16		1.31 ± 1.75	
D_{13}	-0.27 ± 1.37		1.38 ± 4.97		0.13 ± 1.87	
D_{14}	0.65 ± 1.35		-4.18 ± 4.83		1.68 ± 1.85	

Table IV. Type of terms present in each $C_i(M^2)$ and D_i. The J and $\mathcal{J}$ values have been suppressed. For example, $\langle pS|pS\rangle$ includes the following terms: $|(pS_{1/2})_{1/2}|^2$, $|(pS_{1/2})_{3/2}|^2$, and $\langle(pS_{1/2})_{1/2}|(pS_{1/2})_{3/2}\rangle$. The terms in column b (the shaded region) become zero under the choice of amplitudes made in Section V.

	(a)	(b)
C_1	$\|sS\|^2$, $\Sigma\|sP\|^2$, $\Sigma\|pS\|^2$,	$\Sigma\|pP\|^2$
C_2	$\langle sS\|pS\rangle$,	$\langle sP\|pP\rangle$
C_3	$\langle sS\|sP\rangle$,	$\langle pS\|pP\rangle$
C_4	$\langle pS\|sP\rangle$,	$\langle sS\|pP\rangle$
C_5	$\langle pS\|sP\rangle$,	$\langle sS\|pP\rangle$
C_6	$\langle pS\|pS\rangle$,	$\langle pP\|pP\rangle$
C_7	$\langle sP\|sP\rangle$,	$\langle pP\|pP\rangle$
C_8		$\langle pS\|pP\rangle$
C_9		$\langle pS\|pP\rangle$
C_{10}		$\langle sP\|pP\rangle$
C_{11}		$\langle sP\|pP\rangle$
C_{12}		$\langle pP\|pP\rangle$
C_{13}		$\langle pP\|pP\rangle$
C_{14}		$\langle pP\|pP\rangle$

Table V. Partial cross sections and percentages of the four partial waves present in the reaction

$\pi p \rightarrow \pi p \eta$

	1050-MeV/c π^+	1170-MeV/c π^+	1170-MeV/c π^-
$(sS_{1/2})_{1/2}$	2.2 μb 24 ± 7%	6.7 μb 13 ± 4%	10.8 μb 67 ± 3%
$(sP_{3/2})_{3/2}$	5.6 μb 59 ± 6%	39.0 μb 73 ± 7%	4.5 μb 27 ± 4%
$(pS_{1/2})_{1/2}$	1.2 μb 13 ± 3%	5.0 μb 9 ± 2%	0.6 μb 4 ± 1%
$(pS_{1/2})_{3/2}$	0.5 μb 4 ± 1%	2.6 μb 5 ± 1%	0.3 μb 2 ± $\frac{1}{2}$%

Table AI. The ten possible states resulting from s- and p-wave eta and π-p production and S- and P-wave decay of the π-p system.

Final state $(\ell\, L_J)_\vartheta$	Initial state $\mathcal{L}_\vartheta$
$(sS_{1/2})_{1/2}$	$\mathcal{P}_{1/2}$
$(sP_{1/2})_{1/2}$	$\mathcal{S}_{1/2}$
$(sP_{3/2})_{3/2}$	$\mathcal{D}_{3/2}$
$(pS_{1/2})_{1/2}$	$\mathcal{S}_{1/2}$
$(pS_{1/2})_{3/2}$	$\mathcal{D}_{3/2}$
$(pP_{1/2})_{1/2}$	$\mathcal{P}_{1/2}$
$(pP_{1/2})_{3/2}$	$\mathcal{P}_{3/2}$
$(pP_{3/2})_{1/2}$	$\mathcal{P}_{1/2}$
$(pP_{3/2})_{3/2}$	$\mathcal{P}_{3/2}$
$(pP_{3/2})_{5/2}$	$\mathcal{F}_{5/2}$

Table AII. Definition of the $C_i(M^2)$'s and D_i's in terms of the a's. The shaded terms are zero under the choice of amplitudes made in Section V.

C_1	$\|a_{00}\|^2 + \|a_{01}\|^2 + 2\|a_{03}\|^2 + \|a_{10}\|^2 + 2\|a_{30}\|^2$ $+ \|a_{11}\|^2 + 2\|a_{31}\|^2 + \|a_{13}\|^2 + 2\|a_{33}\|^2 + 3\|a_{53}\|^2$
C_2	$\frac{2}{\sqrt{3}}\langle a_{00}\|(a_{10} + 2a_{30})\rangle$ $+ \frac{2}{3\sqrt{3}}\langle(a_{01} + 2a_{03})\|(a_{11} + 2a_{31}) - \sqrt{2}\,[a_{13} + (\frac{2}{5})^{1/2} a_{33} - 3(\frac{3}{5})^{1/2} a_{53}]\rangle$ $+ \frac{4}{9}\langle(a_{01} - a_{03}\|(a_{11} + 2a_{31}) + \frac{1}{\sqrt{2}}[a_{13} + (\frac{2}{5})^{1/2} a_{33} - 3(\frac{3}{5})^{1/2} a_{53}]\rangle$
C_3	$\frac{2}{\sqrt{3}}\langle a_{00}\|(a_{01} + 2a_{03})\rangle$ $+ \frac{2}{3\sqrt{3}}\langle(a_{10} + 2a_{30})\|(a_{11} + 2a_{31}) - \sqrt{2}\,[a_{13} + (\frac{2}{5})^{1/2} a_{33} - 3(\frac{3}{5})^{1/2} a_{53}]\rangle$ $+ \frac{4}{9}\langle(a_{10} - a_{30})\|(a_{11} - a_{31}) + \frac{1}{\sqrt{2}}[a_{13} + 4(\frac{2}{5})^{1/2} a_{33} + 3(\frac{3}{5})^{1/2} a_{53}]\rangle$
C_4	$\frac{2}{3}\langle(a_{10} + 2a_{30})\|(a_{01} + 2a_{03})\rangle$ $+ \frac{2}{3}\langle a_{00}\|(a_{11} + 2a_{31}) - \sqrt{2}\,[a_{13} + (\frac{2}{5})^{1/2} a_{33} - 3(\frac{3}{5})^{1/2} a_{53}]\rangle$
C_5	$-\frac{4}{3}\langle(a_{10} - a_{30})\|(a_{01} - a_{03})\rangle$ $+ \frac{4}{3}\langle a_{00}\|(a_{11} - a_{31}) - \frac{1}{2\sqrt{2}}[a_{13} + 4(\frac{2}{5})^{1/2} a_{33} + 3(\frac{3}{5})^{1/2} a_{53}]\rangle$ $- \sqrt{2}\langle a_{00}\|[a_{13} - 2(\frac{2}{5})^{1/2} a_{33} + 3(\frac{3}{5})^{1/2} a_{53}]\rangle$
C_6	$\frac{2}{3(5)^{1/2}}\|(a_{10} + 2a_{30})\|^2 - \frac{2}{3(5)^{1/2}}\|(a_{10} - a_{30})\|^2$ $+ \frac{2}{9(5)^{1/2}}\|(a_{11} + 2a_{31}) - \sqrt{2}\,[a_{13} + (\frac{2}{5})^{1/2} a_{33} - 3(\frac{3}{5})^{1/2} a_{53}]\|^2$ $- \frac{4}{9(5)^{1/2}}\|(a_{11} - a_{31}) - \frac{1}{2\sqrt{2}}[a_{13} + 4(\frac{2}{5})^{1/2} a_{33} + 3(\frac{3}{5})^{1/2} a_{53}]\|^2$ $+ \frac{4}{9(5)^{1/2}}\|(a_{11} + 2a_{31}) + \frac{1}{\sqrt{2}}[a_{13} + (\frac{2}{5})^{1/2} a_{33} - 3(\frac{3}{5})^{1/2} a_{53}]\|^2$ $- \frac{2}{9(5)^{1/2}}\|(a_{11} - a_{31}) + \frac{1}{\sqrt{2}}[a_{13} + 4(\frac{2}{5})^{1/2} a_{33} + 3(\frac{3}{5})^{1/2} a_{53}]\|^2$ $- \frac{1}{2(5)^{1/2}}\|[a_{13} - 2(\frac{2}{5})^{1/2} a_{33} + 3(\frac{3}{5})^{1/2} a_{53}]\|^2$
C_7	$\frac{2}{3(5)^{1/2}}\|(a_{01} + 2a_{03})\|^2 - \frac{2}{3(5)^{1/2}}\|(a_{01} - a_{03})\|^2$ $+ \frac{2}{9(5)^{1/2}}\|(a_{11} + 2a_{31}) - \sqrt{2}\,[a_{13} + (\frac{2}{5})^{1/2} a_{33} - 3(\frac{3}{5})^{1/2} a_{53}]\|^2$ $- \frac{4}{9(5)^{1/2}}\|(a_{11} - a_{31}) - \frac{1}{2\sqrt{2}}[a_{13} + 4(\frac{2}{5})^{1/2} a_{33} + 3(\frac{3}{5})^{1/2} a_{53}]\|^2$ $- \frac{2}{9(5)^{1/2}}\|(a_{11} + 2a_{31}) + \frac{1}{\sqrt{2}}[a_{13} + (\frac{2}{5})^{1/2} a_{33} - 3(\frac{3}{5})^{1/2} a_{53}]\|^2$ $+ \frac{4}{9(5)^{1/2}}\|(a_{11} - a_{31}) + \frac{1}{\sqrt{2}}[a_{13} + 4(\frac{2}{5})^{1/2} a_{33} + 3(\frac{3}{5})^{1/2} a_{53}]\|^2$ $- \frac{1}{2(5)^{1/2}}\|[a_{13} - 2(\frac{2}{5})^{1/2} a_{33} + 3(\frac{3}{5})^{1/2} a_{53}]\|^2$

Table AII. (cont.)

C_8	$\frac{4}{3(15)^{1/2}}\langle(a_{10}+2a_{30})\|(a_{11}+2a_{31})-\sqrt{2}[a_{13}+(\frac{2}{5})^{1/2}a_{33}-3(\frac{3}{5})^{1/2}a_{53}]\rangle$ $-\frac{4}{9(5)^{1/2}}\langle(a_{10}-a_{30})\|(a_{11}-a_{31})+\frac{1}{\sqrt{2}}[a_{13}+4(\frac{2}{5})^{1/2}a_{33}+3(\frac{3}{5})^{1/2}a_{53}]\rangle$
C_9	$\frac{4}{3(5)^{1/2}}\langle(a_{10}+2a_{30})\|(a_{11}-a_{31})-\frac{1}{2\sqrt{2}}[a_{13}+4(\frac{2}{5})^{1/2}a_{33}+3(\frac{3}{5})^{1/2}a_{53}]\rangle$ $-\frac{4}{9}(\frac{3}{5})^{1/2}\langle(a_{10}-a_{30})\|(a_{11}+2a_{31})+\frac{1}{\sqrt{2}}[a_{13}+(\frac{2}{5})^{1/2}a_{33}-3(\frac{3}{5})^{1/2}a_{53}]\rangle$ $-\frac{2}{10^{1/2}}\langle(a_{10}+2a_{30})\|[a_{13}-2(\frac{2}{5})^{1/2}a_{33}+3(\frac{3}{5})^{1/2}a_{53}]\rangle$
C_{10}	$\frac{4}{3(15)^{1/2}}\langle(a_{01}+2a_{03})\|(a_{11}+2a_{31})-\sqrt{2}[a_{13}+(\frac{2}{5})^{1/2}a_{33}-3(\frac{3}{5})^{1/2}a_{53}]\rangle$ $-\frac{4}{9(5)^{1/2}}\langle(a_{01}-a_{03})\|(a_{11}+2a_{31})+\frac{1}{\sqrt{2}}[a_{13}+(\frac{2}{5})^{1/2}a_{33}-3(\frac{3}{5})^{1/2}a_{53}]\rangle$
C_{11}	$\frac{4}{3(5)^{1/2}}\langle(a_{01}+2a_{03})\|(a_{11}-a_{31})-\frac{1}{2\sqrt{2}}[a_{13}+4(\frac{2}{5})^{1/2}a_{33}+3(\frac{3}{5})^{1/2}a_{53}]\rangle$ $-\frac{4}{9}(\frac{3}{5})^{1/2}\langle(a_{01}-a_{03})\|(a_{11}-a_{31})+\frac{1}{\sqrt{2}}[a_{13}+4(\frac{2}{5})^{1/2}a_{33}+3(\frac{3}{5})^{1/2}a_{53}]\rangle$ $-\frac{2}{10^{1/2}}\langle(a_{01}+2a_{03})\|[a_{13}-2(\frac{2}{5})^{1/2}a_{33}+3(\frac{3}{5})^{1/2}a_{53}]\rangle$
C_{12}	$\frac{4}{45}\|(a_{11}+2a_{31})-\sqrt{2}[a_{13}+(\frac{2}{5})^{1/2}a_{33}-3(\frac{3}{5})^{1/2}a_{53}]\|^2$ $+\frac{4}{45}\|(a_{11}+2a_{31})+\frac{1}{\sqrt{2}}[a_{13}+(\frac{2}{5})^{1/2}a_{33}-3(\frac{3}{5})^{1/2}a_{53}]\|^2$ $+\frac{4}{45}\|(a_{11}-a_{31})-\frac{1}{2\sqrt{2}}[a_{13}+4(\frac{2}{5})^{1/2}a_{33}+3(\frac{3}{5})^{1/2}a_{53}]\|^2$ $+\frac{4}{45}\|(a_{11}-a_{31})+\frac{1}{\sqrt{2}}[a_{13}+4(\frac{2}{5})^{1/2}a_{33}+3(\frac{3}{5})^{1/2}a_{53}]\|^2$ $+\frac{1}{10}\|[a_{13}-2(\frac{2}{5})^{1/2}a_{33}+3(\frac{3}{5})^{1/2}a_{53}]\|^2$
C_{13}	$\frac{4}{15}\langle(a_{11}+2a_{31})-\sqrt{2}[a_{13}+(\frac{2}{5})^{1/2}a_{33}-3(\frac{3}{5})^{1/2}a_{53}]\|$ $\|(a_{11}-a_{31})-\frac{1}{2\sqrt{2}}[a_{13}+4(\frac{2}{5})^{1/2}a_{33}+3(\frac{3}{5})^{1/2}a_{53}]\rangle$ $-\frac{4}{15}\langle(a_{11}+2a_{31})+\frac{1}{\sqrt{2}}[a_{13}+(\frac{2}{5})^{1/2}a_{33}-3(\frac{3}{5})^{1/2}a_{53}]\|$ $\|(a_{11}-a_{31})+\frac{1}{\sqrt{2}}[a_{13}+4(\frac{2}{5})^{1/2}a_{33}+3(\frac{3}{5})^{1/2}a_{53}]\rangle$ $-\frac{\sqrt{2}}{5}\langle(a_{11}+2a_{31})-\sqrt{2}[a_{13}+(\frac{2}{5})^{1/2}a_{33}-3(\frac{3}{5})^{1/2}a_{53}]\|$ $\|[a_{13}-2(\frac{2}{5})^{1/2}a_{33}+3(\frac{3}{5})^{1/2}a_{53}]\rangle$
C_{14}	$-\frac{4\sqrt{2}}{5}\langle(a_{11}-a_{31})-\frac{1}{2\sqrt{2}}[a_{13}+4(\frac{2}{5})^{1/2}a_{33}+3(\frac{3}{5})^{1/2}a_{53}]\|$ $\|[a_{13}-2(\frac{2}{5})^{1/2}a_{33}+3(\frac{3}{5})^{1/2}a_{53}]\rangle$

FIGURE CAPTIONS

Fig. 1. Schematic diagram of the beam optics. A mass spectrometer, not shown in the diagram, is used in the π^+ beam to separate π^+ mesons from protons.

Fig. 2. The distributions in the missing neutral mass (using unfitted quantities) for all 4-prongs which fit either of the reactions $\pi^\pm p \to \pi^\pm p\pi^+\pi^-$ (π^0 or γ) with a $\chi^2 < 8.6$.

a. 1170-MeV/c incident π^+.

b. 1050-MeV/c incident π^+.

c. 1170-MeV/c incident π^-.

Fig. 3. The 2C χ^2 distribution of the 273 events for reaction (3) (solid lines). The dashed lines represent the "theoretical" 2C χ^2 distribution normalized to 273 events.

Fig. 4. The distributions in the invariant mass of the $\pi^+\pi^-\pi^0$ (using unfitted quantities) for events in Fig. 2 for which M^2 (missing neutral) > 0.010 BeV^2. There are two pions of the same charge in the final state; only that combination of M^2 ($\pi^+\pi^-\pi^0$) which is closer to $M_\eta^2 = 0.30$ BeV^2 has been plotted.

a. 1170-MeV/c incident π^+.

b. 1050-MeV/c incident π^+.

c. 1170-MeV/c incident π^-.

Fig. 5. Variation of $\sigma(\pi^\pm p \to \pi^\pm p\eta;\ \eta \to \pi^+\pi^-\pi^0)$ as a function of incident beam momentum. The π^+ data points are indicated by black dots; the π^- data points by open circles. See Table II for references. The u = 0 curve is the result of the threshold parameteriza-

tion of the π^+ data (see Section VB). The other solid curves are the results of the modified parameterization of Section VC. The dashed curve is the u = 67 curve for the π^- data.

Fig. 6. Mnemonic (nonrelativistic) diagram in velocity space depicting the two-step reaction $\pi_B p_T \to \eta \tilde{N}$; $\tilde{N} \to \pi_D p_D$. In the overall center of mass π_B has orbital angular momentum $\underset{\sim}{\mathcal{L}}$ and linear momentum $\underset{\sim}{k}$ along the z axis; η has orbital angular momentum $\underset{\sim}{\ell}$ and linear momentum $\underset{\sim}{p}$. The two vectors, $\underset{\sim}{k}$ and $\underset{\sim}{p}$, define the production plane. The normal to the production plane, $\hat{k} \times \hat{p}$, is the y axis; $\hat{x} = \hat{y} \times \hat{z}$. In the $\tilde{N}$ rest frame the z axis is in the production plane at an angle ξ from the line of flight of the eta; $\cos \xi = \hat{p} \cdot \hat{k}$. The $\tilde{N}$ of mass M and total angular momentum $\underset{\sim}{J}$ decays into π_D and p_D with orbital angular momentum $\underset{\sim}{L}$ and linear momentum $\underset{\sim}{q}$; $\cos \theta = \hat{q} \cdot \hat{z}$, $\phi = \tan^{-1} [\hat{q} \cdot \hat{n} / \hat{q} \cdot \hat{x}]$. The total angular momentum of the system is $\underset{\sim}{\mathcal{J}}$; the total energy is E.

Fig. 7. Production Dalitz plots and mass-squared projections. The curves are given by Eqs. (15) and (16), using our best fit parameters.

a. 1170-MeV/c incident π^+.

b. 1050-MeV/c incident π^+.

c. 1170-MeV/c incident π^-.

Fig. 8. Production angular distributions in the center of mass. The curves are given by Eq. (12), using our best fit parameters.

a. 1170-MeV/c incident π^+.

b. 1050-MeV/c incident π^+.

c. 1170-MeV/c incident π^-.

Fig. 9. $\tilde{N}$ azimuthal decay angular distributions. The curves are given by Eq. (13), using our best fit parameters.

a. 1170-MeV/c incident π^+

b. 1050-MeV/c incident π^+.

c. 1170-MeV/c incident π^-.

Fig. 10. $\tilde{N}$ polar decay angular distributions. The curves are given by Eq. (14), using our best fit parameters.

a. 1170-MeV/c incident π^+.

b. 1050-MeV/c incident π^+.

c. 1170-MeV/c incident π^-.

Fig. 11. Mass and angular distributions for the reaction $\pi^+ p \to \pi^+ p\eta$ published in Refs. 2-7. The curves are those given by our parameterization of Section VC, and are normalized to the total number of events.

a. Mass distributions.

b. Angular distributions.

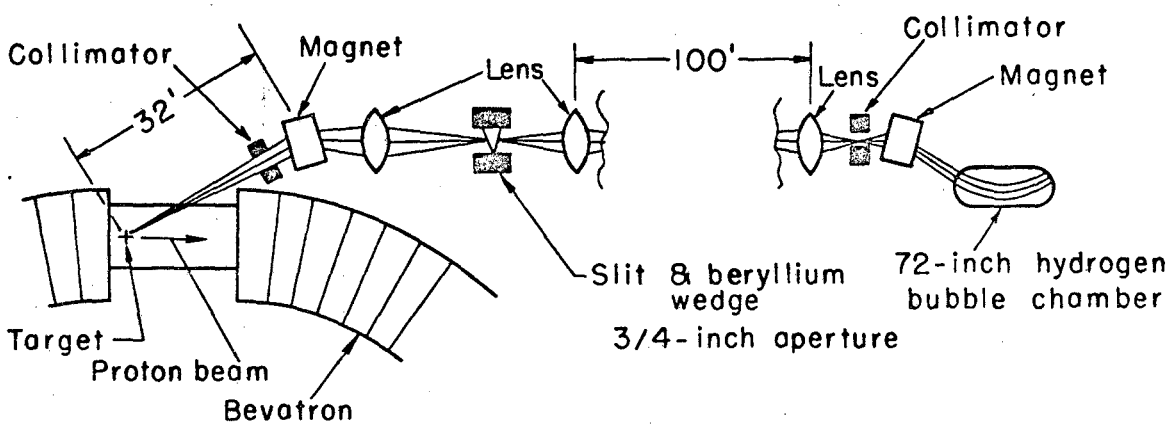
Collimator
Magnet
Lens
100'
Collimator
Lens
Magnet
32'
Slit & beryllium wedge
3/4-inch aperture
72-inch hydrogen bubble chamber
Target
Proton beam
Bevatron
MU-26415

Fig. 1

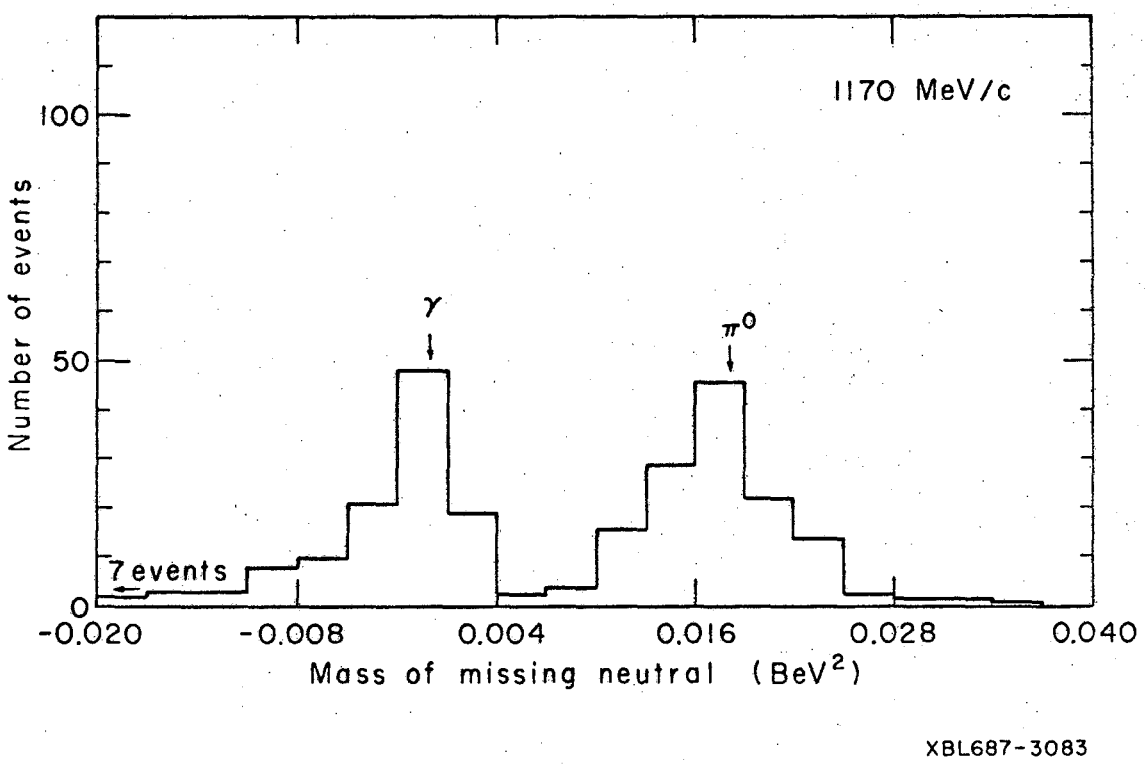
1170 MeV/c
100
50
0
Number of events
γ
π⁰
7 events
-0.020
-0.008
0.004
0.016
0.028
0.040
Mass of missing neutral (BeV²)
XBL687-3083

Fig. 2a

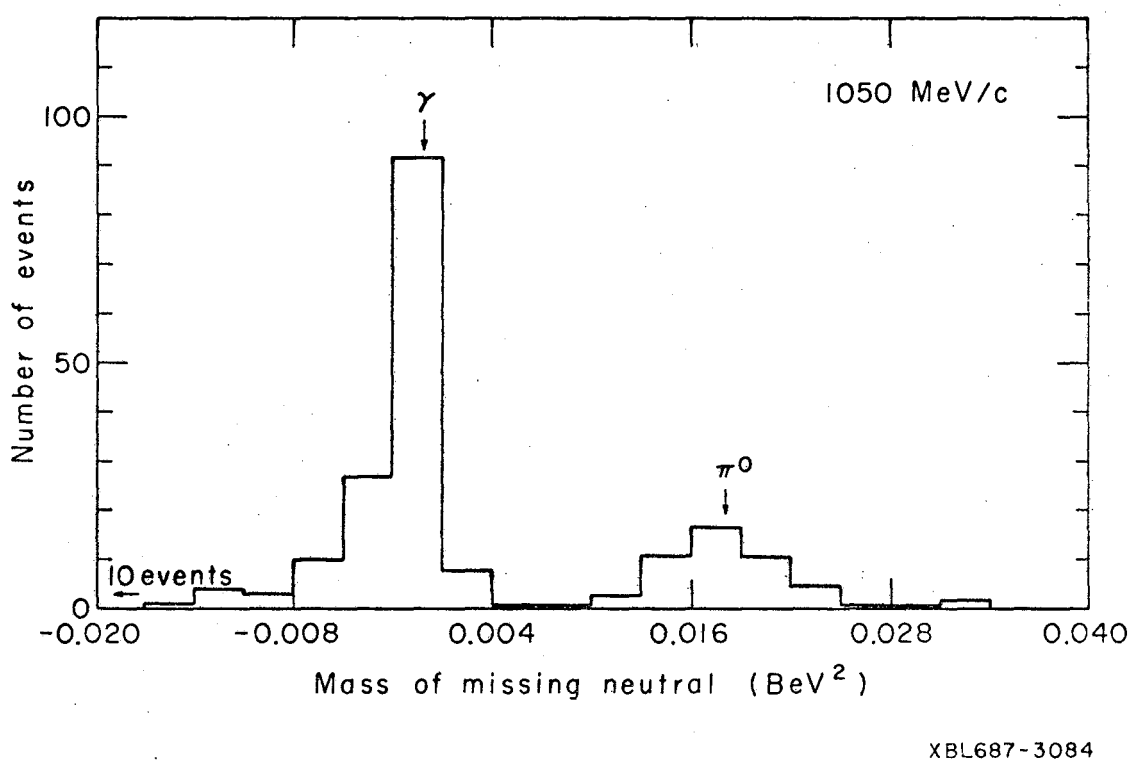
1050 MeV/c
γ
π⁰
100
50
0
10 events
Number of events
-0.020
-0.008
0.004
0.016
0.028
0.040
Mass of missing neutral (BeV²)
XBL687-3084

Fig. 2b

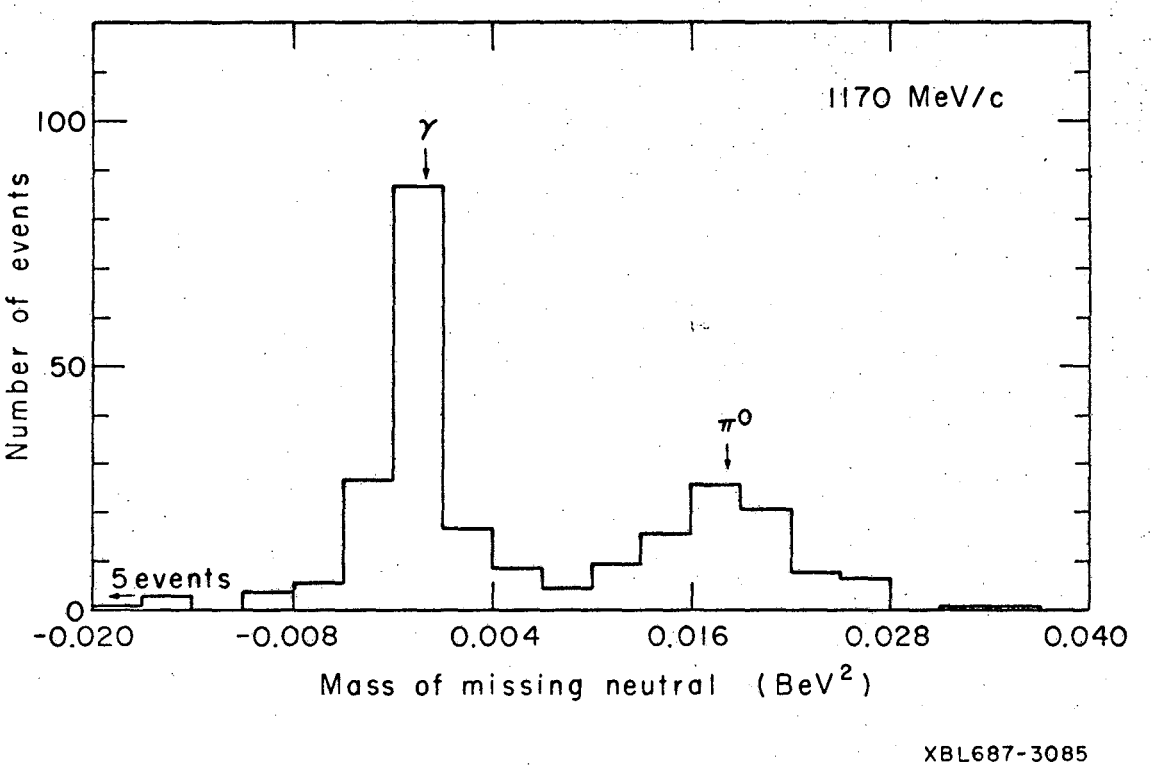
1170 MeV/c
γ
π⁰
100
50
0
Number of events
5 events
-0.020
-0.008
0.004
0.016
0.028
0.040
Mass of missing neutral (BeV²)
XBL687-3085

Fig. 2c

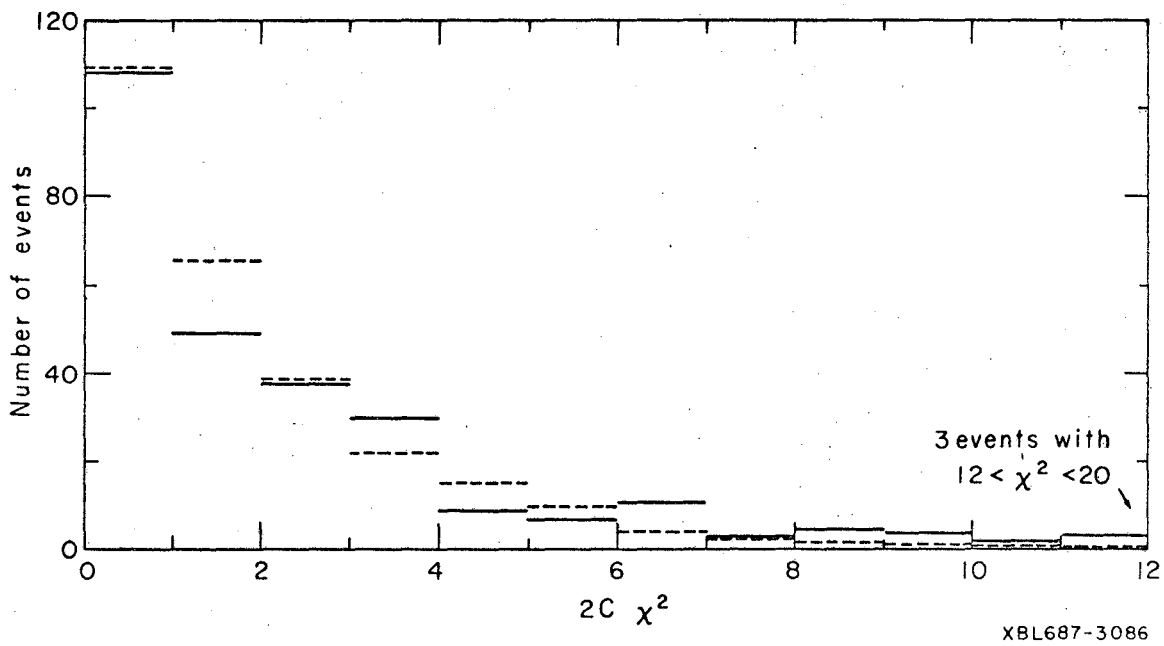
120
80
40
0
Number of events
0
2
4
6
8
10
12
2C χ²
3 events with
12 < χ² <20
XBL687-3086

Fig. 3

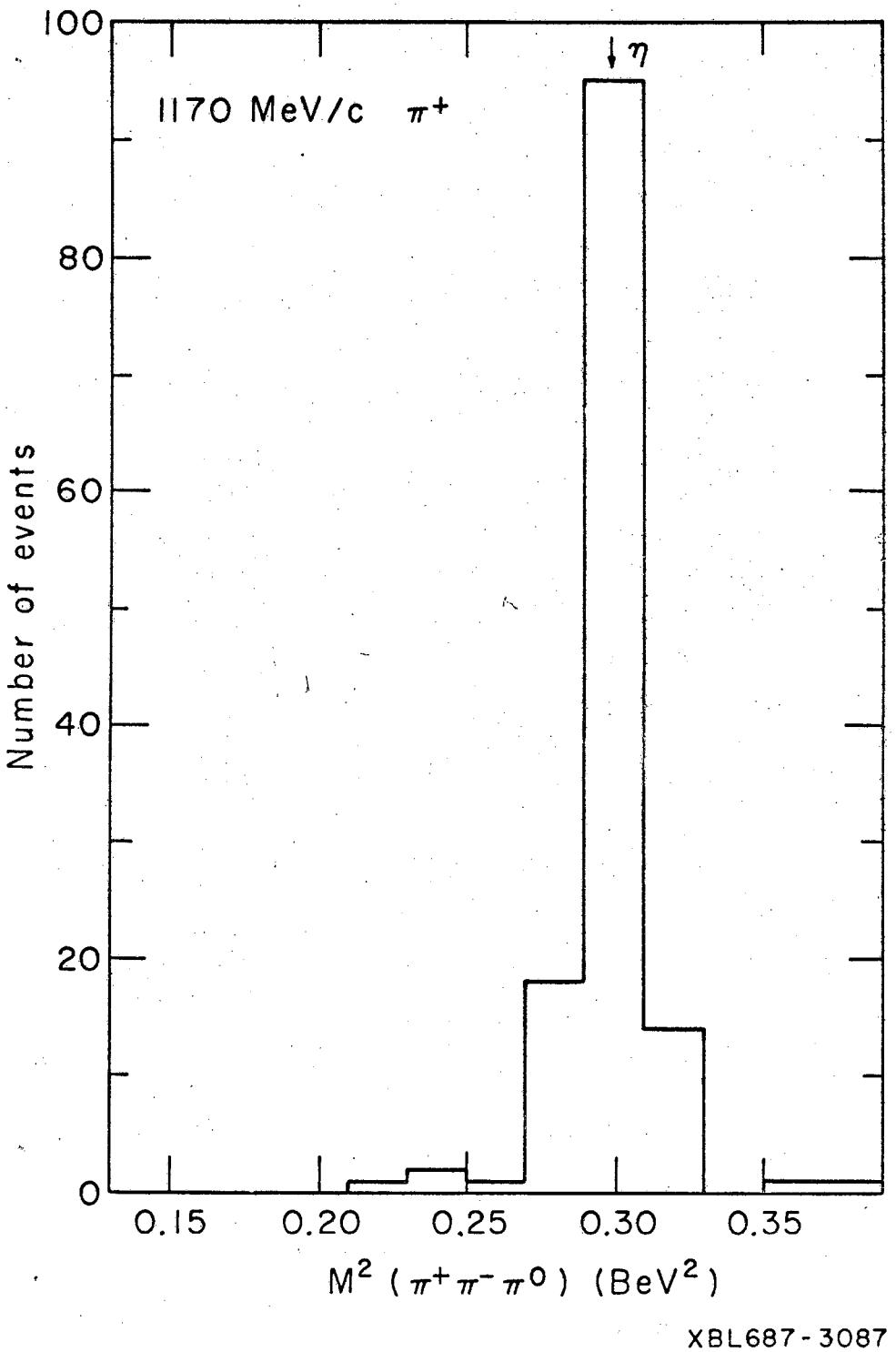
1170 MeV/c π+
η
Number of events
100
80
60
40
20
0
0.15
0.20
0.25
0.30
0.35
M² (π+π−π0) (BeV²)
XBL687-3087

Fig. 4a

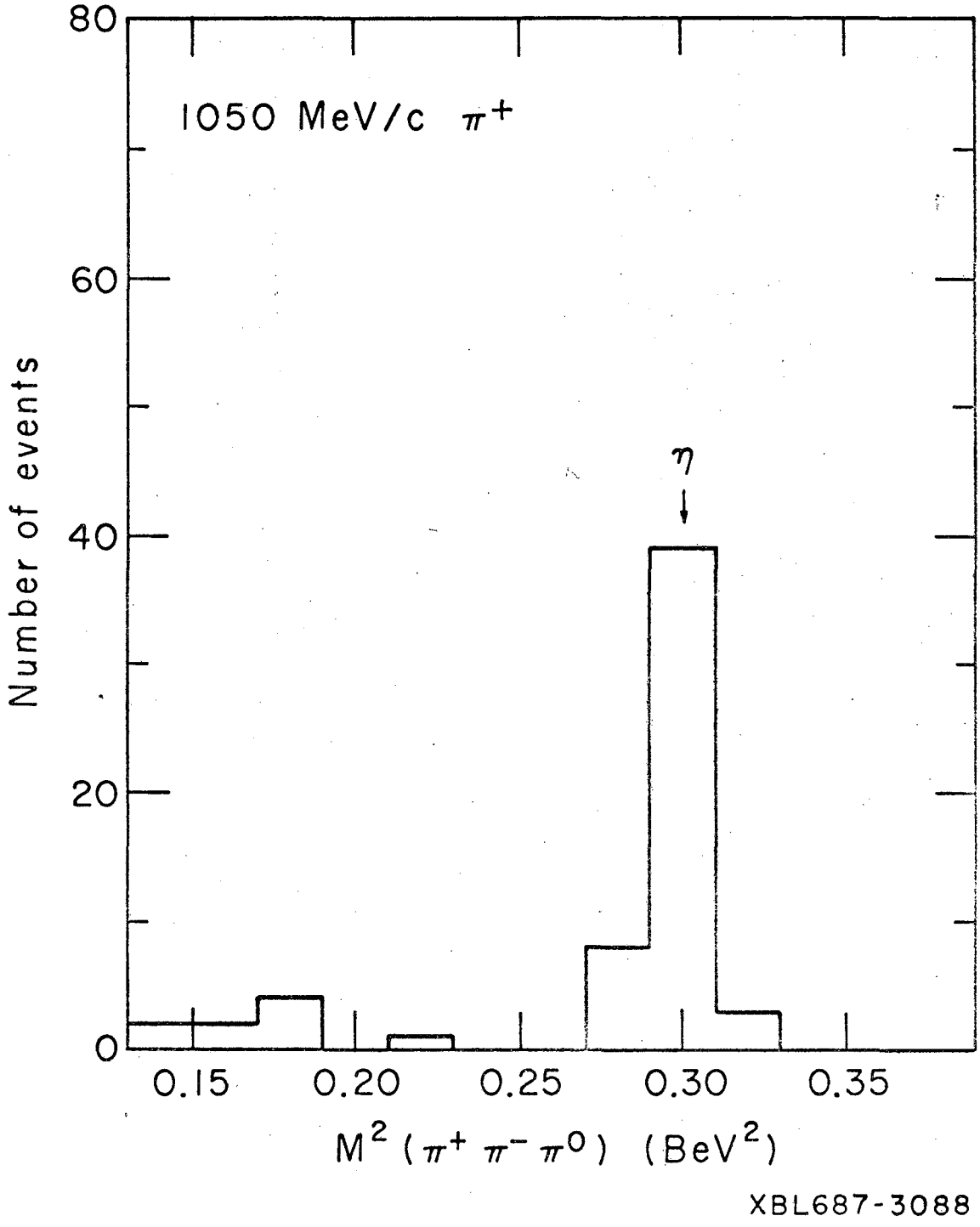
80
60
40
20
0
1050 MeV/c π^+
η
Number of events
0.15
0.20
0.25
0.30
0.35
$M^2(\pi^+\pi^-\pi^0)$ (BeV^2)
XBL687-3088

Fig. 4b

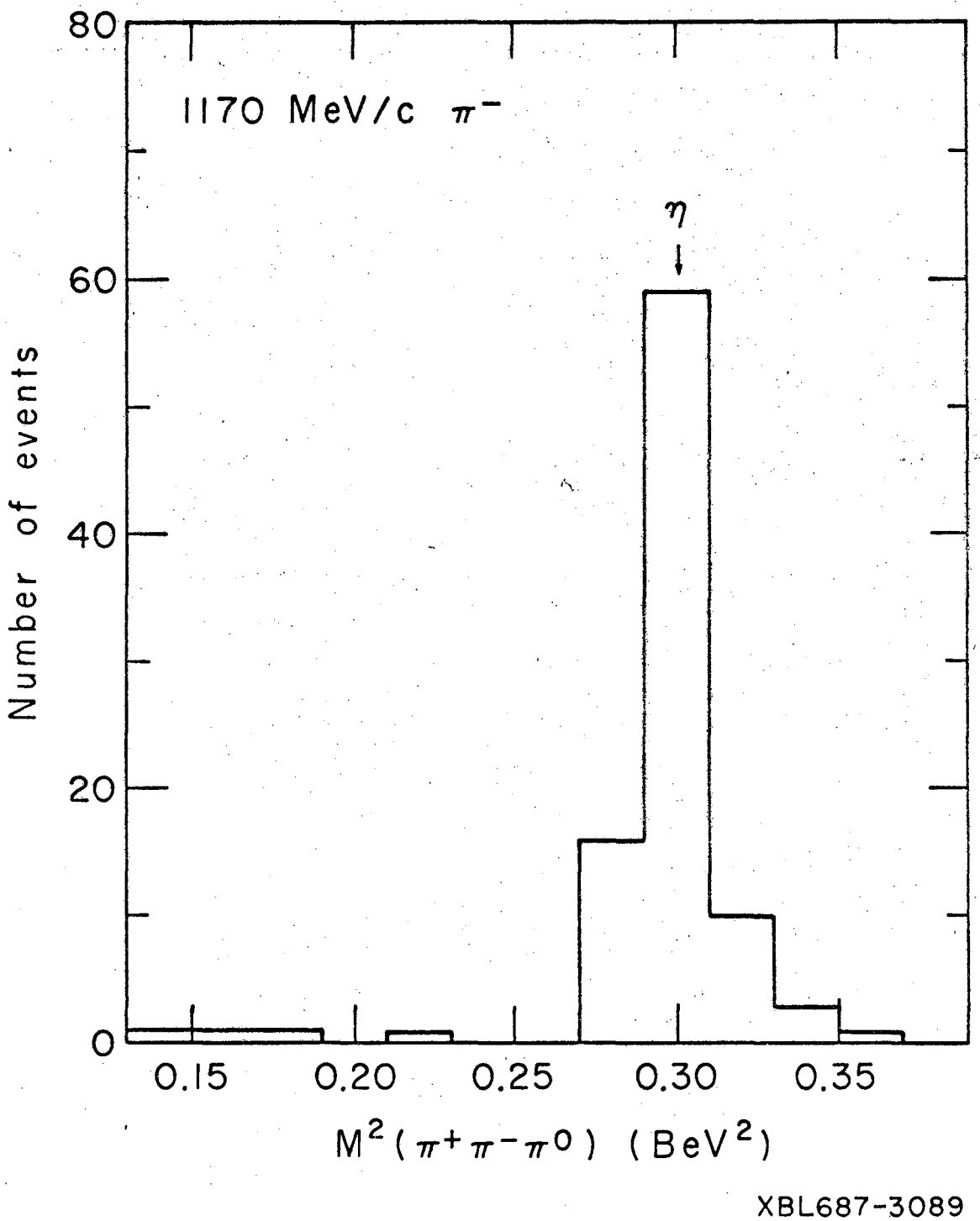
1170 MeV/c π⁻
η
Number of events
80
60
40
20
0
0.15
0.20
0.25
0.30
0.35
M²(π⁺π⁻π⁰) (BeV²)
XBL687-3089

Fig. 4c

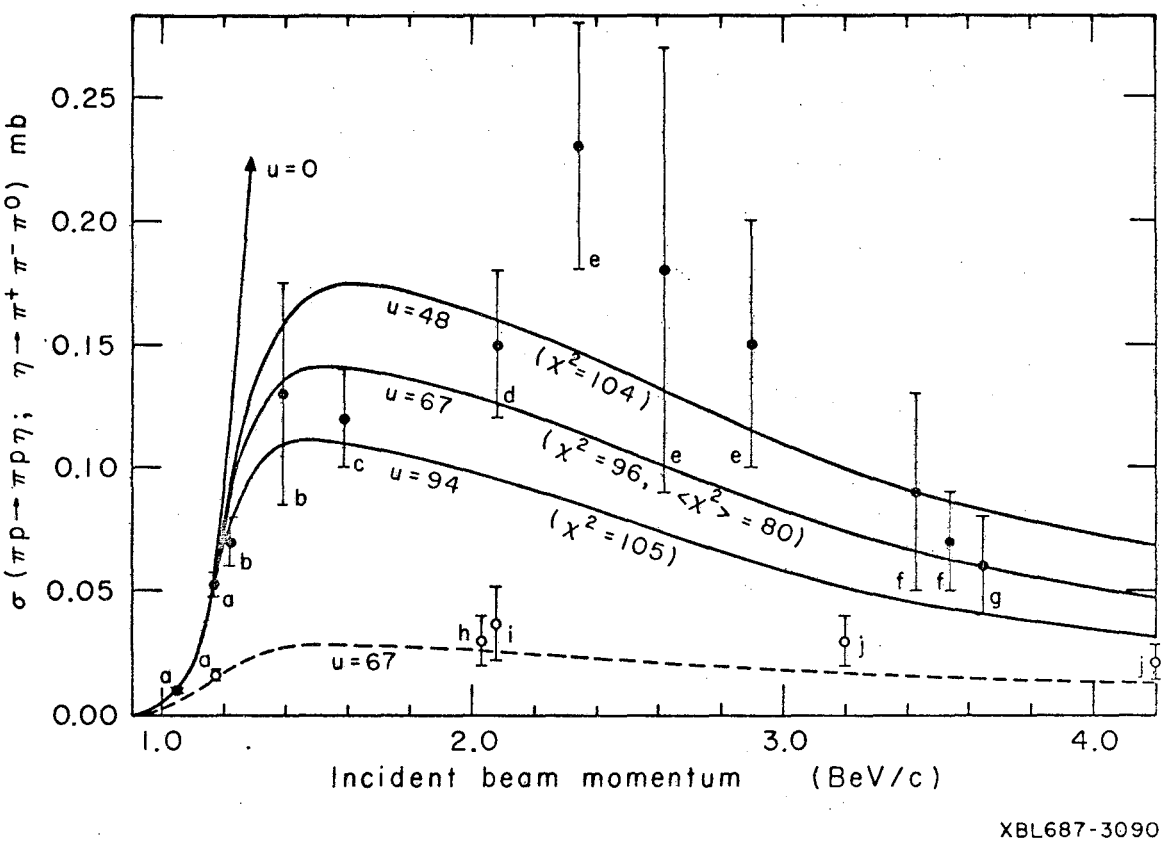
σ (πp → πpη; η → π⁺π⁻π⁰) mb
0.25
0.20
0.15
0.10
0.05
0.00
1.0
2.0
3.0
4.0
Incident beam momentum (BeV/c)
u=0
u=48
(χ²=104)
u=67
(χ²=96, <χ²> = 80)
u=94
(χ²=105)
u=67
a
b
c
d
e
f
g
h
i
j
XBL687-3090

Fig. 5

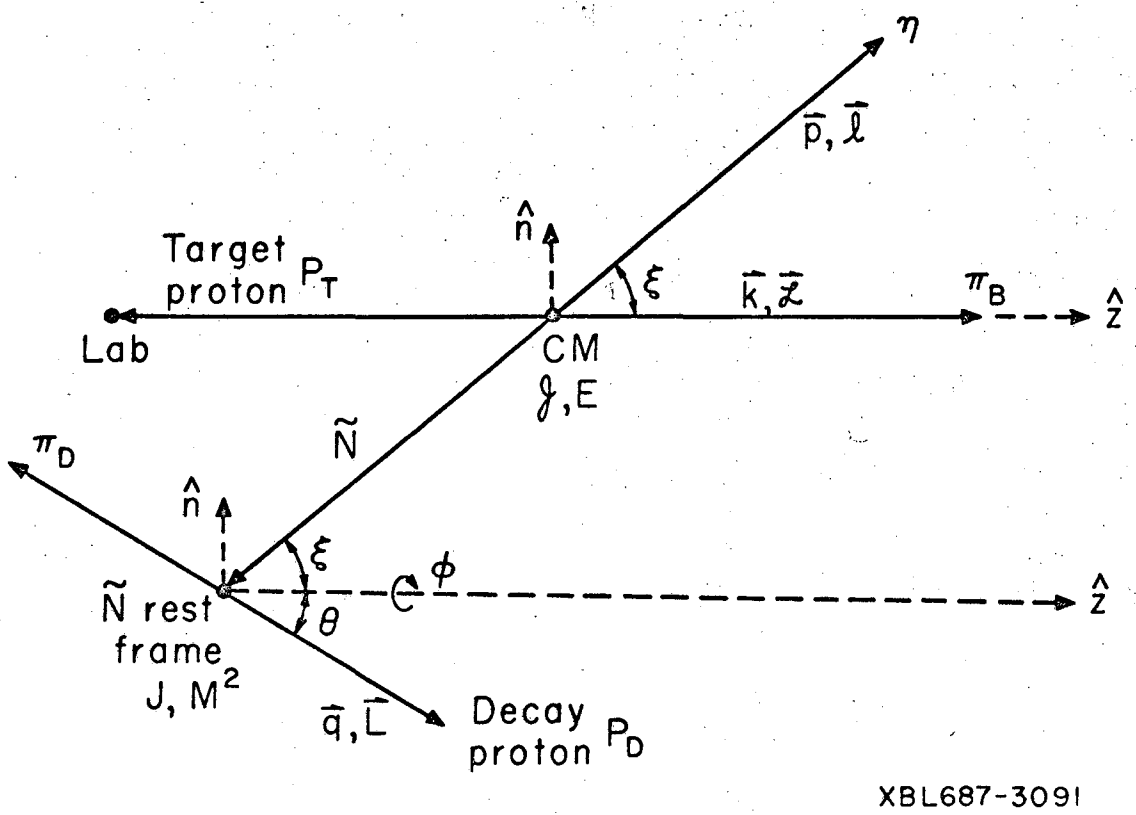
η
p, ℓ
n̂
Target proton P_T
ξ
k, z
π_B
ẑ
Lab
CM
J, E
π_D
Ñ
n̂
ξ
φ
ẑ
Ñ rest frame
J, M²
θ
q, L
Decay proton P_D
XBL687-3091

Fig. 6

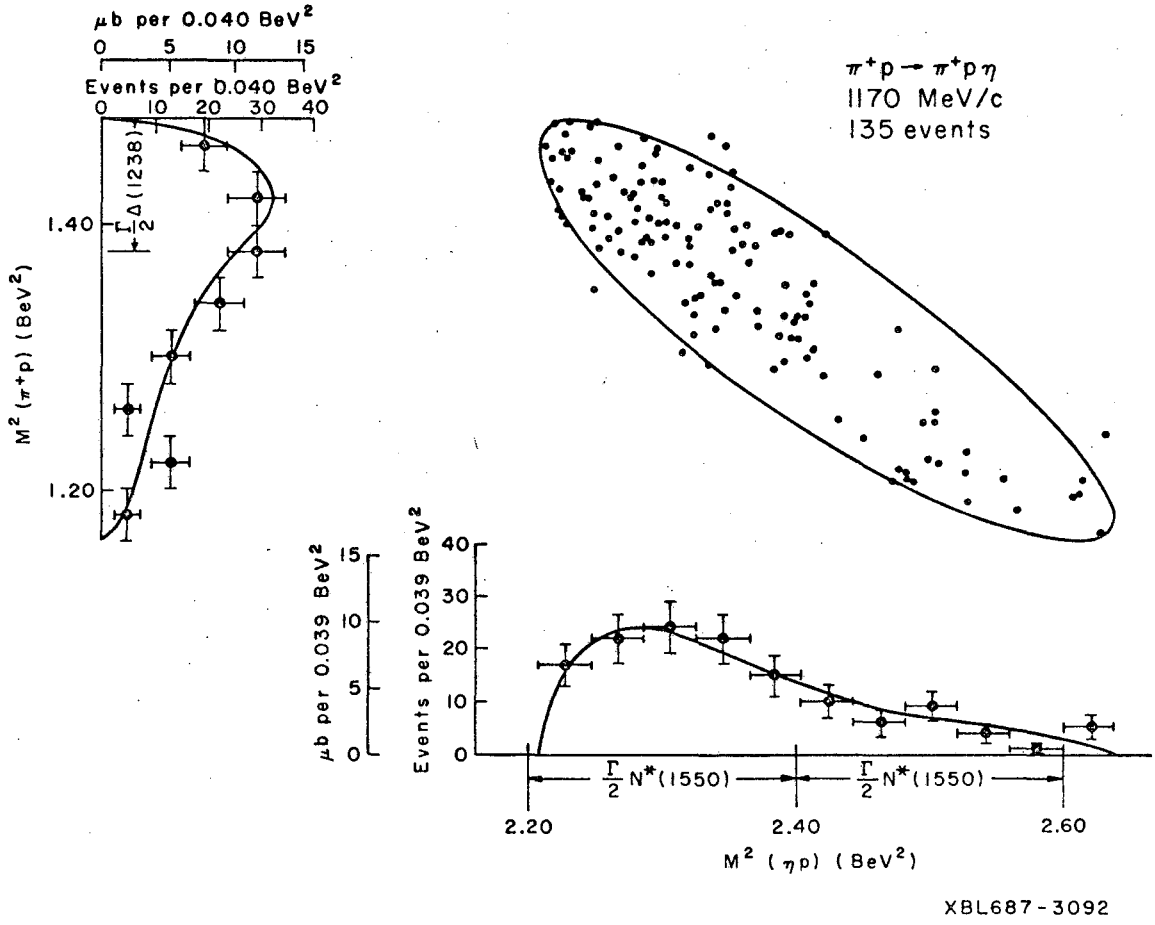
μb per 0.040 BeV²
0 5 10 15
Events per 0.040 BeV²
0 10 20 30 40
Γ/2 Δ(1238)
1.40
1.20
M² (π⁺p) (BeV²)
π⁺p → π⁺pη
1170 MeV/c
135 events
μb per 0.039 BeV²
15 10 5 0
Events per 0.039 BeV²
40 30 20 10 0
Γ/2 N*(1550)
Γ/2 N*(1550)
2.20
2.40
2.60
M² (ηp) (BeV²)
XBL687-3092

Fig. 7a

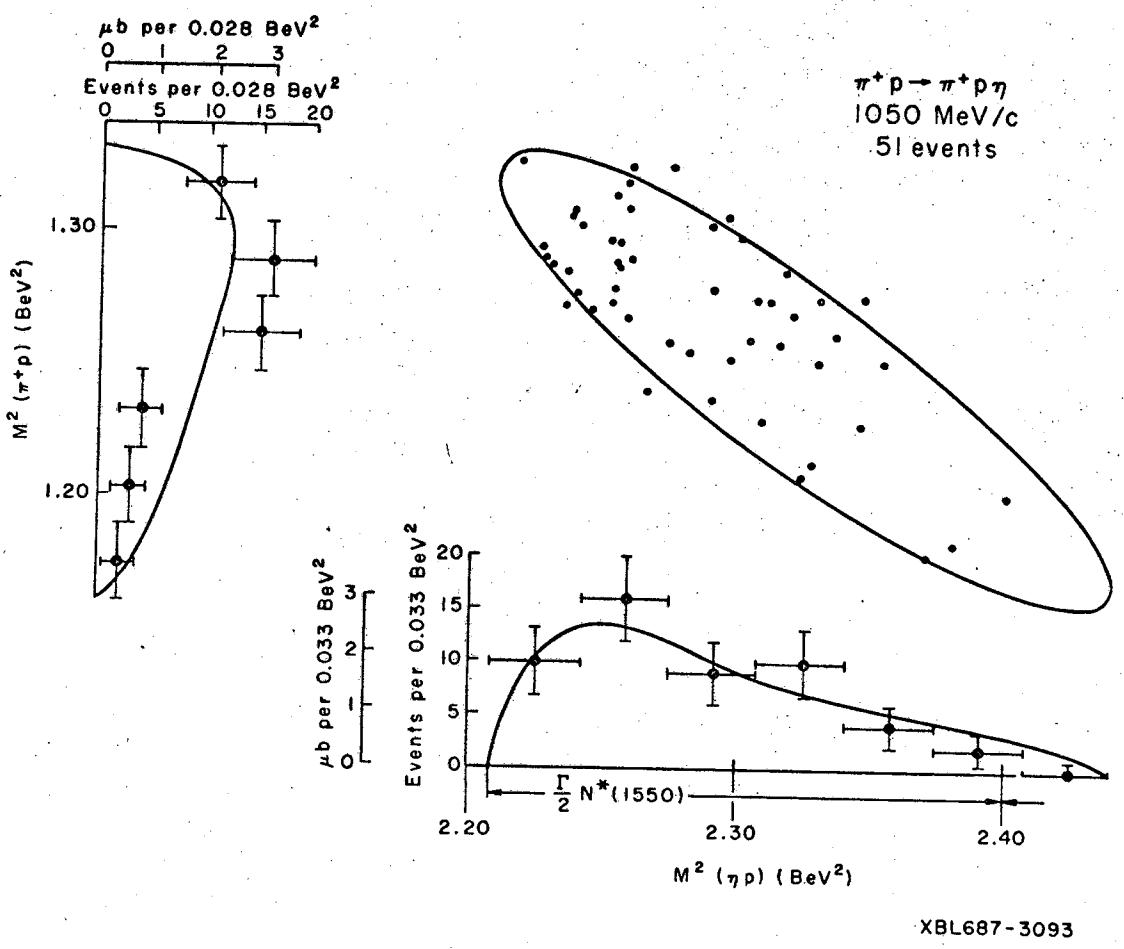
μb per 0.028 BeV²
0 1 2 3
Events per 0.028 BeV²
0 5 10 15 20
1.30
1.20
M² (π⁺p) (BeV²)
π⁺p → π⁺pη
1050 MeV/c
51 events
μb per 0.033 BeV²
3 2 1 0
Events per 0.033 BeV²
20 15 10 5 0
Γ/2 N*(1550)
2.20
2.30
2.40
M² (ηp) (BeV²)
XBL687-3093

Fig. 7b

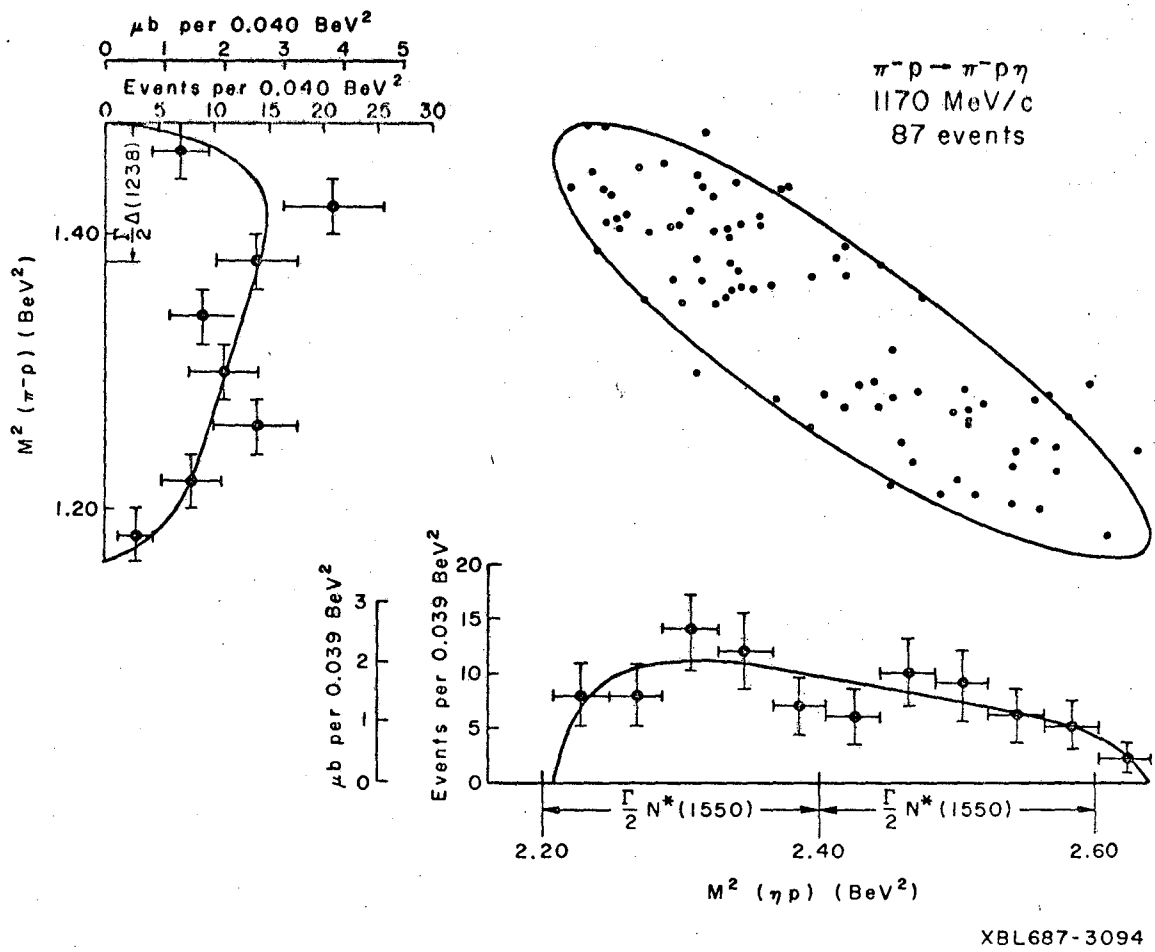
μb per 0.040 BeV²
0 1 2 3 4 5
Events per 0.040 BeV²
0 5 10 15 20 25 30
1.40
1.20
M² (π-p) (BeV²)
Γ/2 Δ(1238)
π⁻p → π⁻pη
1170 MeV/c
87 events
μb per 0.039 BeV²
3
2
1
0
Events per 0.039 BeV²
20
15
10
5
0
Γ/2 N*(1550)
Γ/2 N*(1550)
2.20
2.40
2.60
M² (ηp) (BeV²)
XBL687-3094

Fig. 7c

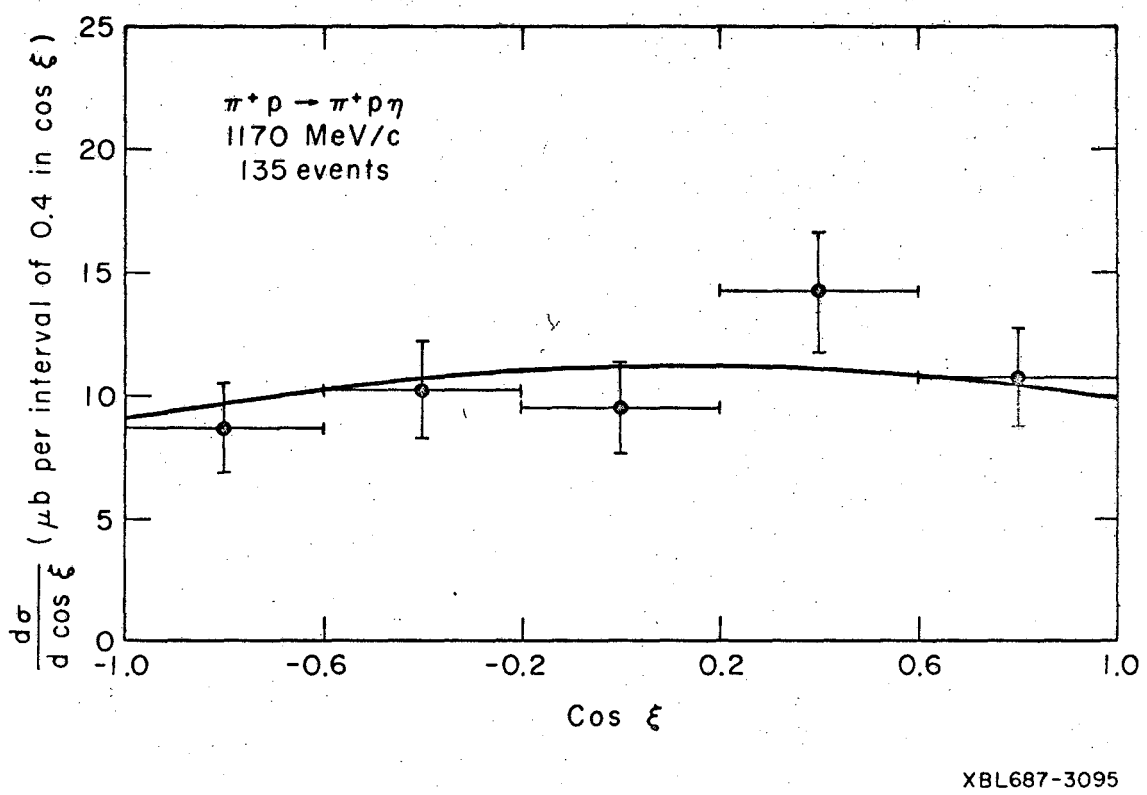
$\pi^+ p \rightarrow \pi^+ p \eta$
1170 MeV/c
135 events
$\frac{d\sigma}{d \cos \xi}$ (μb per interval of 0.4 in cos ξ)
25
20
15
10
5
0
-1.0
-0.6
-0.2
0.2
0.6
1.0
Cos ξ
XBL687-3095

Fig. 8a

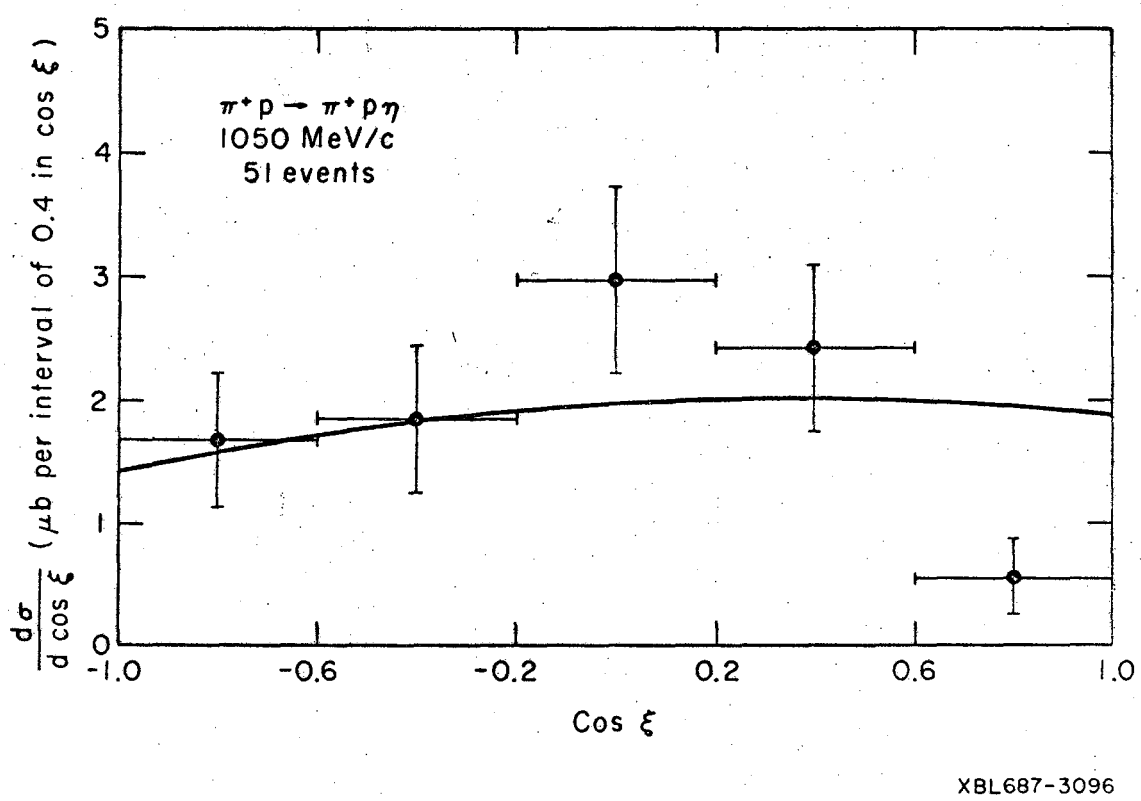
$\pi^+ p \rightarrow \pi^+ p \eta$
1050 MeV/c
51 events
$\frac{d\sigma}{d \cos \xi}$ (μb per interval of 0.4 in cos ξ)
Cos ξ
0
1
2
3
4
5
-1.0
-0.6
-0.2
0.2
0.6
1.0
XBL687-3096

Fig. 8b

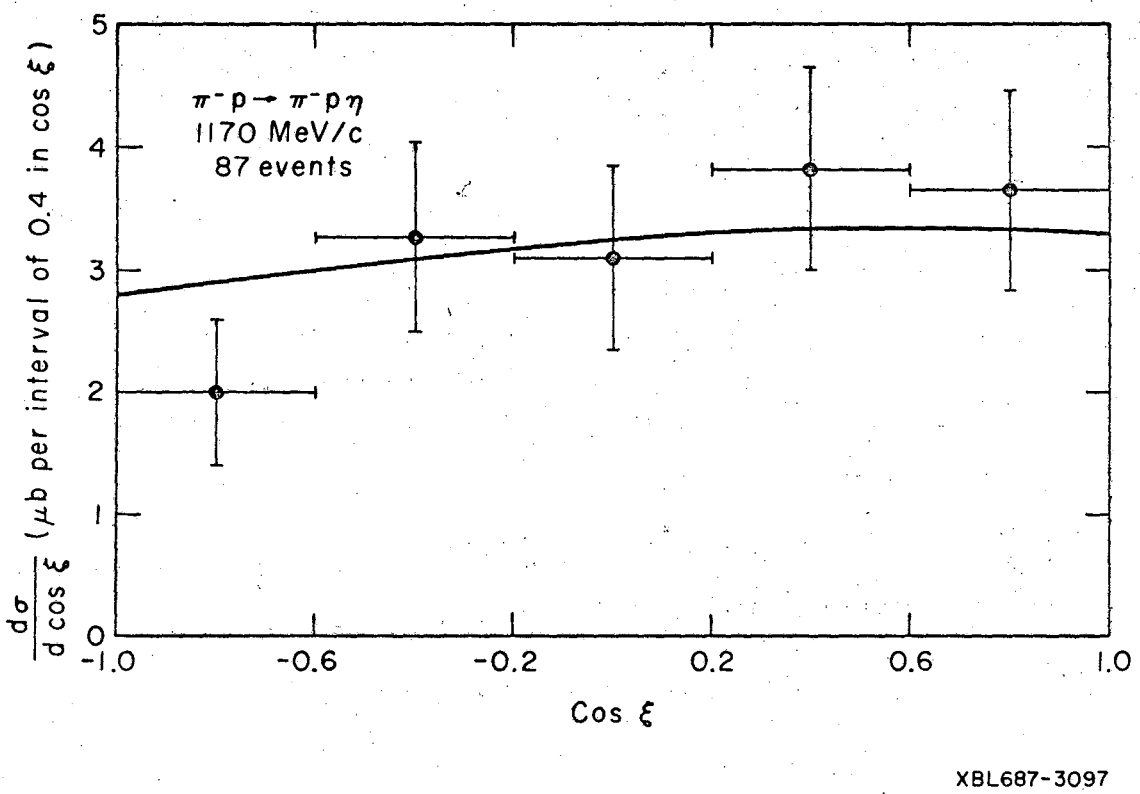
$\pi^- p \rightarrow \pi^- p \eta$
1170 MeV/c
87 events
$\frac{d\sigma}{d\cos\xi}$ (μb per interval of 0.4 in cos ξ)
Cos ξ
5
4
3
2
1
0
-1.0
-0.6
-0.2
0.2
0.6
1.0
XBL687-3097

Fig. 8c

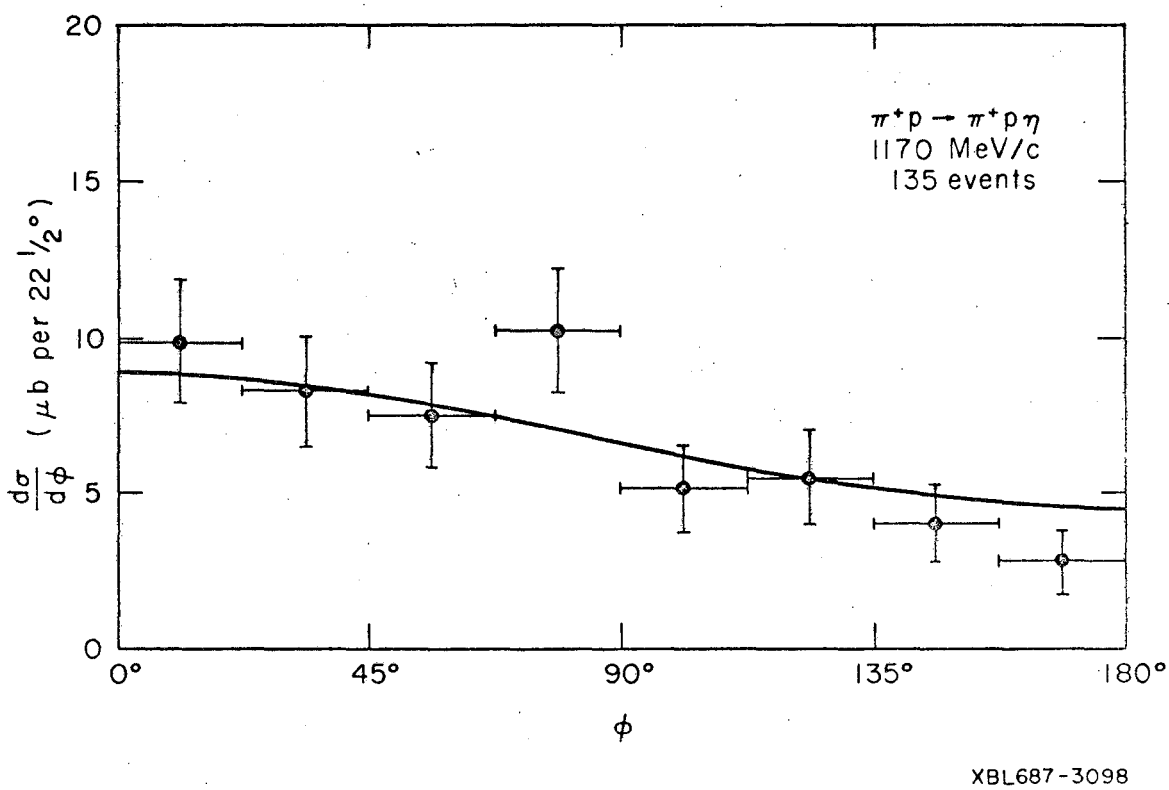
$\pi^+p \rightarrow \pi^+p\eta$
1170 MeV/c
135 events
$\frac{d\sigma}{d\phi}$ (μb per 22 1/2°)
20
15
10
5
0
0°
45°
90°
135°
180°
ϕ
XBL687-3098

Fig. 9a

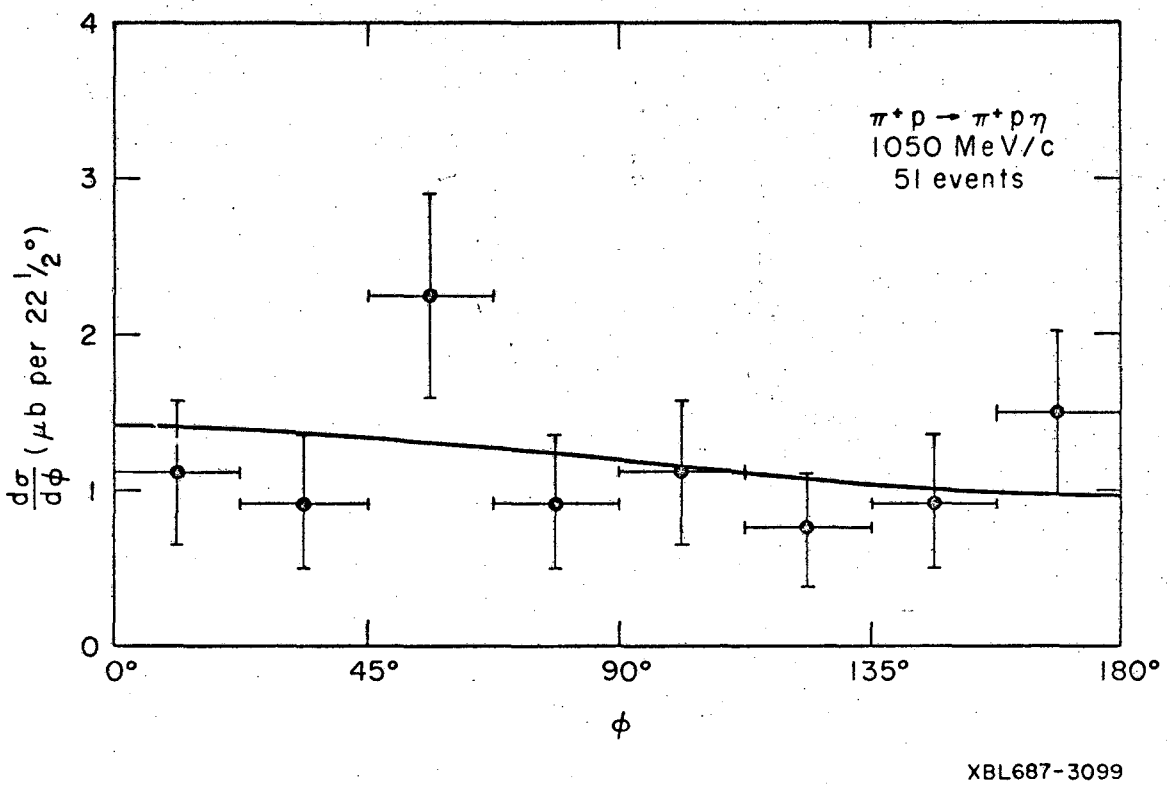
$\pi^+ p \rightarrow \pi^+ p \eta$
1050 MeV/c
51 events
$\frac{d\sigma}{d\phi}$ (μb per 22 1/2°)
0
1
2
3
4
0°
45°
90°
135°
180°
ϕ
XBL687-3099

Fig. 9b

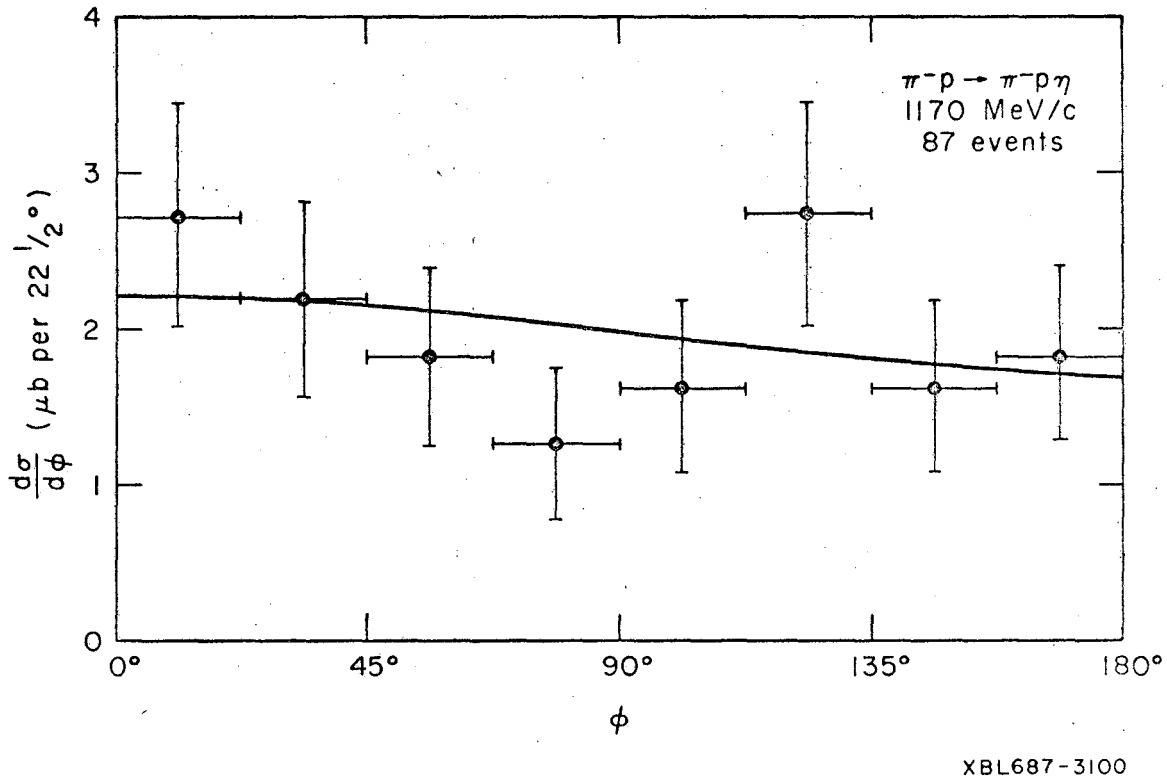
$\pi^- p \rightarrow \pi^- p \eta$
1170 MeV/c
87 events
$\frac{d\sigma}{d\phi}$ (μb per 22 1/2°)
0
1
2
3
4
0°
45°
90°
135°
180°
ϕ
XBL687-3100

Fig. 9c

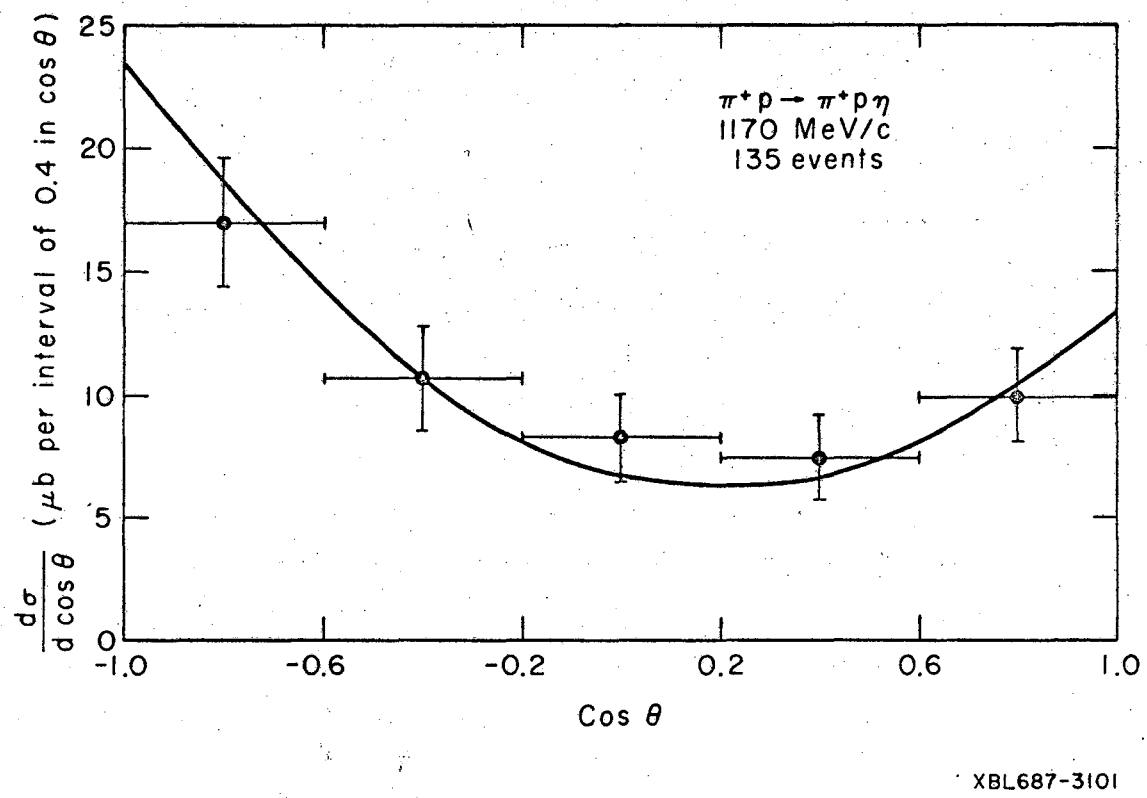
$\pi^+ p \rightarrow \pi^+ p \eta$
1170 MeV/c
135 events
$\frac{d\sigma}{d\cos\theta}$ (μb per interval of 0.4 in cos θ)
25
20
15
10
5
0
-1.0
-0.6
-0.2
0.2
0.6
1.0
Cos θ
XBL687-3101

Fig. 10a

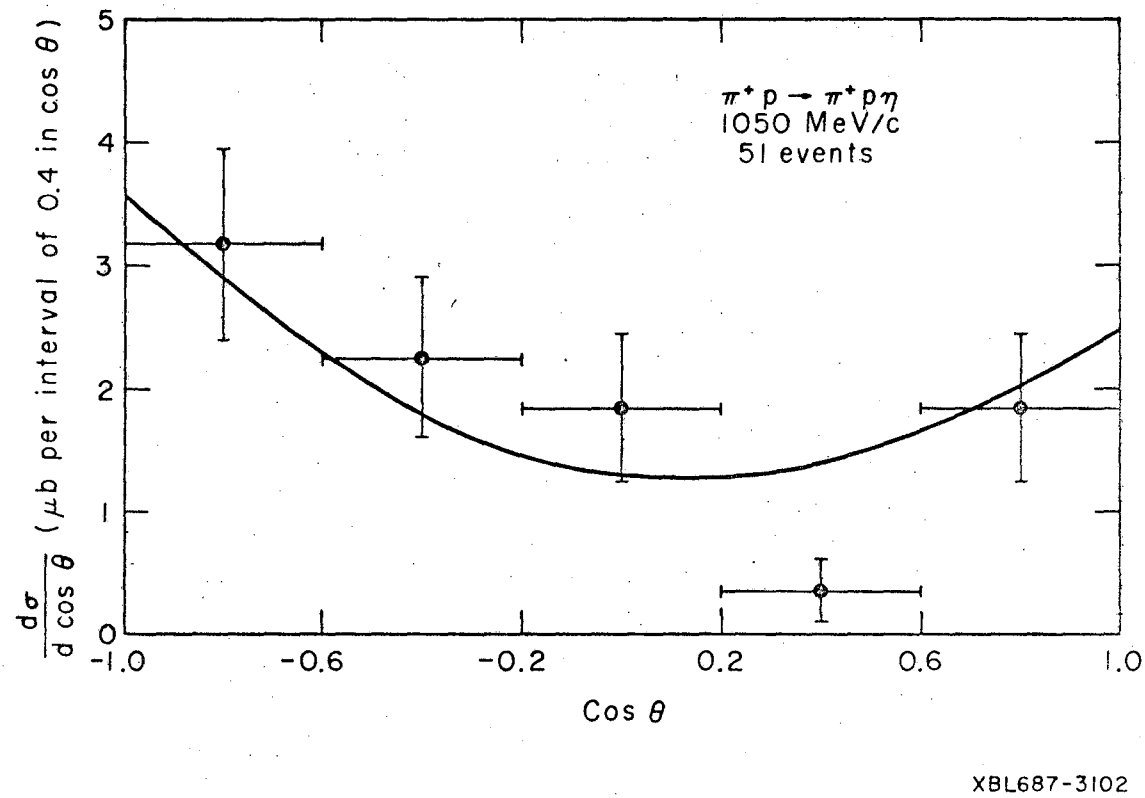
$\pi^+ p \rightarrow \pi^+ p\eta$
1050 MeV/c
51 events
$\frac{d\sigma}{d\cos\theta}$ (μb per interval of 0.4 in cos θ)
Cos θ
5
4
3
2
1
0
-1.0
-0.6
-0.2
0.2
0.6
1.0
XBL687-3102

Fig. 10b